Received: 17 September 2019 | Revised: 1 March 2020 | Accepted: 3 March 2020

DOI: 10.1002/ese3.710

MODELING AND ANALYSIS

Energy Science & Engineering Open Access

# Expander design procedures and selection criterion for small rated organic rankine cycle systems

**Roberto Capata** | **Fabio Pantano**

Department of Mechanical and Aerospace Engineering, University of Roma "Sapienza", Rome, Italy

**Correspondence**
Roberto Capata, Department of Mechanical and Aerospace Engineering, University of Roma "Sapienza", Rome, Italy.
Email: roberto.capata@uiniroma1.it

**Abstract**

The particular aspect of this work is the new approach to expander design procedure for small rated ORC. In fact, once all the calculation procedures have been defined, they have been implemented in Matlab code. This code, once the design process is complete, provides an indication of the optimal expander configuration to adopting to that specific system. For these reasons, this paper aims to analyze all the preliminary expanders' design procedures, both dynamic and volumetric. The reasons lie in the development of low-enthalpy heat recovery systems (systems that allow simultaneous production of electrical and thermal energy made available in the form of water at a temperature of 60-90°C), with the aim of optimizing any energy system. Within these energy systems, the expander is the main component, responsible for power generation. It is, therefore, necessary and useful to analyze in detail every expander configuration, highlighting the different features. For each component will be described the theory on which is based the choice and its design and a possible software implementation is supplied. Finally, a criterion for the choice of the optimal expander is proposed, based on some operational considerations and other construction and structural constraints, such as overall dimensions and weight, lubrication, MTBF, feasibility, reliability, and coupling with the electric generator.

**KEYWORDS**

dynamic expander, expander selection, pistons expander, rotary vane expander, screw expander, scroll expander

## 1 | INTRODUCTION—OVERVIEW AND STATE OF TECHNOLOGY

The expander selection and the optimization of its performance are fundamental in low-temperature heat recovery systems. The parameters that must be considered are high efficiency isentropic, pressure ratio, power, lubrication requirements, complexity, rotation speed, dynamic balancing, reliability, and cost. In these systems, the turboexpanders are not always the optimal solution. For these reasons, taking advantage of all the research in the field of dynamic and volumetric machines, a design procedure for all expander types has been presented.

### 1.1 | Inward-flow radial turbine

The radial flow turbines (IFR) are used in turbochargers for commercial engines and fire pumps. They are very compact

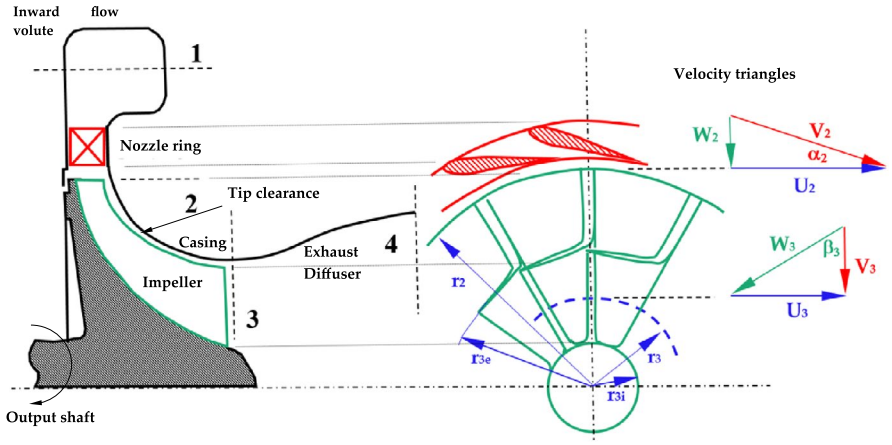


**FIGURE 1** Radial turbine example

and characterized by high rotational speeds. In the inward flow radial turbine, gas enters into the radial direction and leaves it axially as shown in Figure 1. The rotor, which is usually manufactured of cast nickel alloy, presents bent blades to change the flow from the radial to the axial direction.[1,2]

## 1.2 | Scroll

The basic structure of the scroll expander is illustrated in Figure 2. The orbiting scroll is engaged with the fixed scroll from expansion chambers. The high-pressure fluid enters from the center, in the axial direction, and begins to expand in the sealed pockets. This puts the mobile scroll in rotation, which is coupled with an eccentric pin to the crankshaft.[1]

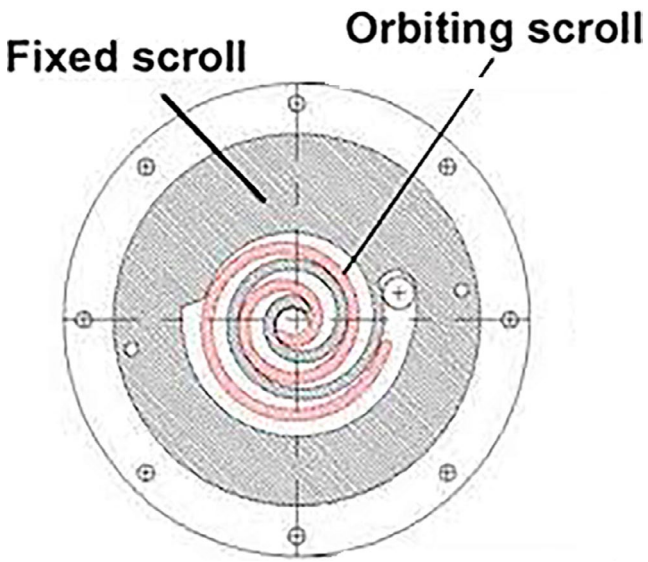


**FIGURE 2** Scroll expander

## 1.3 | Screw expander

Screw expander is comprised of a pair of meshing helical rotors (a "male" and a "female" rotor), as shown in Figure 3, contained in a casing with clearances within 50 μm. As the rotors rotate, the volume trapped between the rotors and the casing changes. If a fluid is admitted into this space, its volume will either increase or decrease, depending only on the direction of rotation, until it is finally expelled at the outlet section. Power is transferred between the fluid and the rotor shafts by pressure on the rotors, which changes with the fluid volume flow rate.[3]

## 1.4 | Vane expander

Rotary vane expanders (RVE) are positive displacement devices that are composed of housing, rotor, vane slots, and vanes, shown in Figure 4. When vapor in high-pressure and high-temperature conditions enters the inlet (1), it starts to expand, causing the rotor to move. As the rotor moves, the expansion volume increases (2 → 3). The volumes are kept isolated by the vanes, which slide out to form a seal and are kept in place by the high pressure behind them,for this reason, to minimize wear and enhance sealing, lubrication is needed. At the end of the expansion, the vapor is exhausted (4). Various positive characteristics can be enumerated such as simple construction, low noise-vibration, high volumetric expansion ratios as large as ten, and wet expansion tolerance.[4] They are also capable of handling high pressures.[5] As there are limited contact surfaces, the friction losses are minimal in the RVE. From various studies,[5,6] it has been noted as the main loss for this type of machine is the leakage. This phenomenon occurs between the vanes and the housing as well as between the ends of the rotor and the sealing faces. Some authors[4] enlighten that the drop in pressure results in an efficiency decrease of up to 65%, while losses account for only 20%. Yang et al.[6] tested a double effect RVE in a steam compression cycle where he replaced the expansion process to improve the COP. Anna et al[5] tested an RVE in an ORC with a source temperature ranging from 60 to

**FIGURE 3** Screw expander example

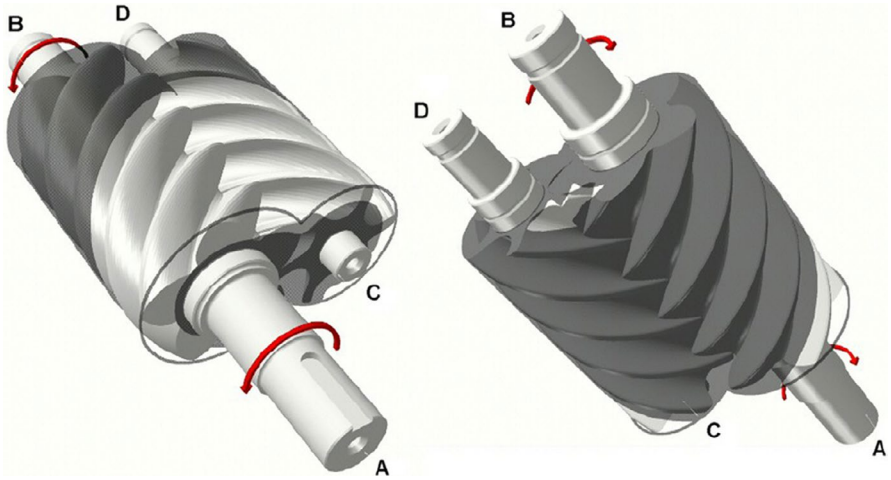


80°C. The RVE achieved a maximum isentropic efficiency of 48% with a power output of 32 W. In Figure 5 operating range for all expanders is shown.

### 1.4.1 | Pistons expanders

Volumetric reciprocating expanders (Figure 6) are suitable for high-pressure ratio. They have a good isentropic efficiency (about 70%) and a good power output/size ratio.[1] Moreover, they are more robust than scroll expanders. Such machinery can be used for a waste heat recovery system. In this type of machine, the steam/organic fluid enters into the cylinder at the inlet pressure ($p_{max}$) and fills it, gradually moving the piston towards the BDC (bottom dead center). Under ideal conditions, it can be assumed that until the introduction of the fluid is interrupted, this phase takes place at constant pressure. Once the admission phase is over, the fluid still has considerable pressure energy (depending on the admission pressure) which allows it to continue to push the plunger, even if of decreasing intensity, expanding within the cylinder up to the discharge pressure. This transformation can be considered adiabatic, neglecting heat exchanges towards the environment. Once the discharge pressure is reached, the fluid is discharged and pushed by the plunger that now advances towards the TDC (top dead center). The discharge takes place continuously and neglecting the passive resistances, it can be assumed that this phase occurs at constant pressure.

Finally, the Balje map is reported in Figure 7, for a complete overview and comparison between the different expanders, here considered. Last considerations. The purpose of this study is to provide a proper tool for choosing an expander for ORC systems. It is also one of the research topics within the industrial sector for optimization and consumption reduction. Finally, this research was sponsored by University Research Funds.

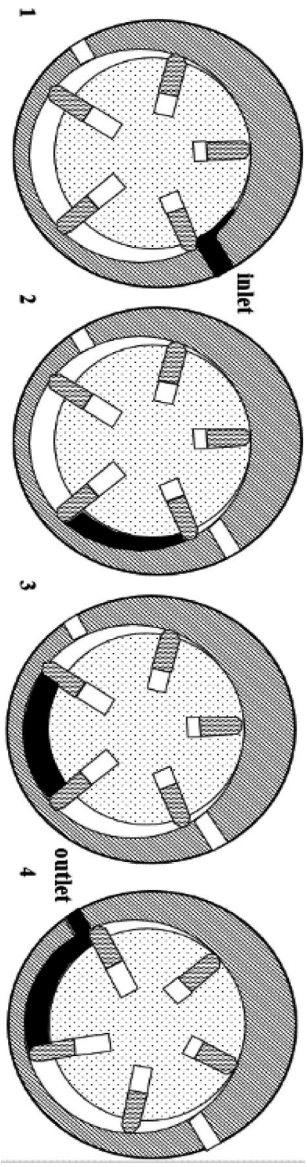


**FIGURE 4** Rotary vane expander

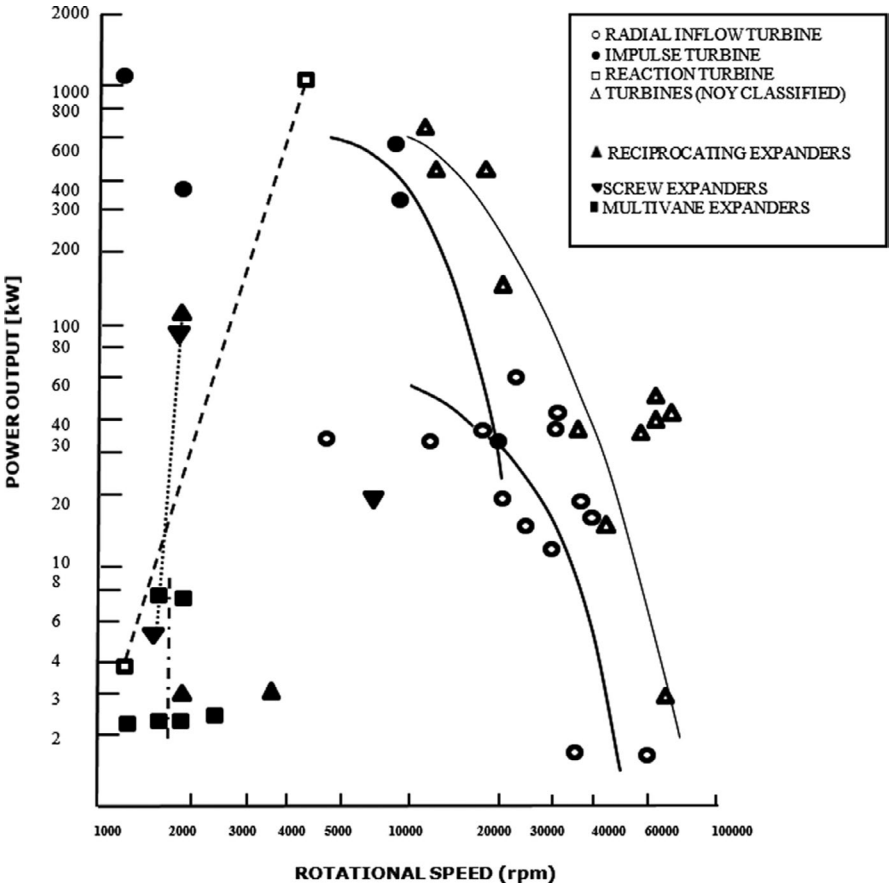


**FIGURE 5** Turbine/expanders use as a function of the rotational speed and the output power[4]

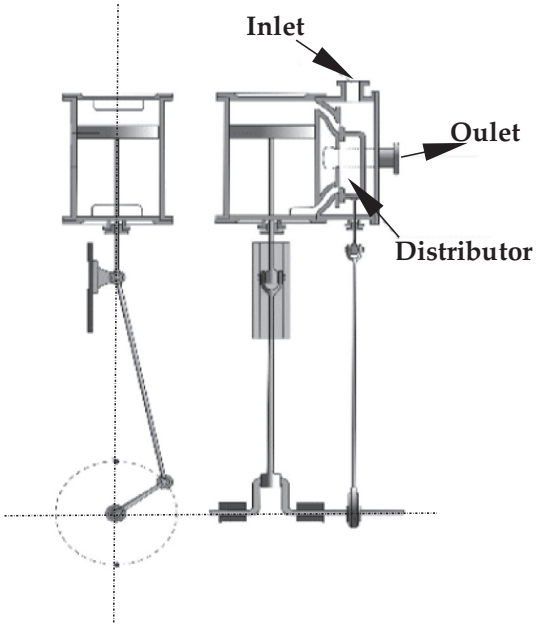


**FIGURE 6** A pistons expanders (PE)

### 1.4.2 | Scope of the paper

After this brief overview, all calculation procedures for expanders' design are studied. These procedures are transcribed in Matlab code. At the design procedure end, the code transcribes all the results on a database. This database becomes the basis of the next part of code that supplies a table by assigning ratings from 1 to 3 (1 *less desirable* 3 *more desirable*) and allowing the user to choose the optimal configuration for the specific ORC system. The choice made by the code is based on various data found in the literature or other research groups and through communications with the expander manufacturers. Moreover, if during the design process, some data or constraints do not allow convergence, the code provides warnings to the user. For this reason, all flow charts of the various procedures are shown. So, once both the required power and the various structural/fluid dynamic constraints are known or assigned, the code gives the designer an indication/suggestion which machine to adopt.

## 2 | TURBO-EXPANDER DESIGN—THE ROHLIK METHOD

Rohlik[2] has analytically studied radial centripetal turbines performance, to determine the optimal geometry for different applications, each one identified by the characteristic parameter called "specific speed" ($\Omega_s$). Five different loss types have been calculated for various combinations

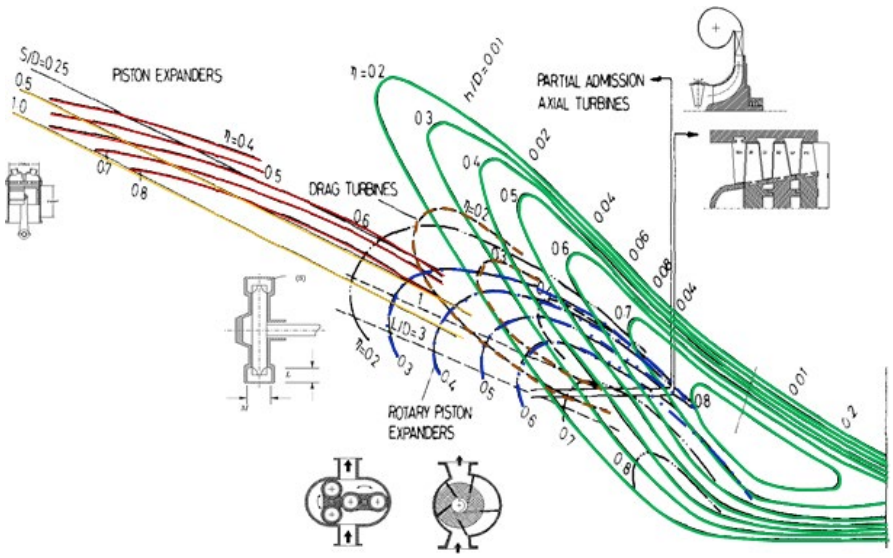


**FIGURE 7** Operating $n_s$ $d_s$ map for different expander from Balje textbook[7]

of parameters: nozzle exit flow angle ($\alpha_1$), diameter ratio between inlet and mid-span outlet section ($D_{2mid}/D_1$), rotor inlet blade height to inlet diameter ratio ($b_1/D_1$), etc The losses considered are:

1. Stator losses.
2. Impeller losses.
3. Tip clearance losses (the gap between impeller and the machine stationary walls to avoid friction losses).
4. Gas leakage on seals.
5. Kinetic energy losses at the outlet.

Obtained results where the efficiencies for a variety of different operating turbines with "Specific Speed ($\Omega_s$)" vary between 0.12 and 1.34. The pressure ratio between upstream and downstream of the turbine had no additional relationship on the definition of parameters for the optimal geometry, except for the vane height. This is because the height of the blade is linked to the density (and consequently to the local pressure) of the fluid evolving in the turbine. The different graphics produced in Rohlik's work are calculated for achieving the maximum efficiency for each value of the specific speed ($\Omega_s$) and allow a quick initial design for every possible application. The radial centripetal turbines are suitable for multiple uses in the field of aeronautics, aerospace, and other areas where compact power sources are needed. This type of turbines is characterized by high efficiency, ease of production and operative reliability. A parameter, widely used in these studies, is the so-called "specific speed ($\Omega_s$)" collects and links various operating parameters such as the rotational speed, volumetric flow and isentropic enthalpy variation (work). These quantities, in most cases, are specified by external conditions: by the pump, or by the compressor or the generator to which the turbine is connected. The definition and the formula of $\Omega_s$ are given further in this paragraph. The Ωs value provides indications of the preliminary geometry for the turbine. At low values, of this parameter, are associated with low passing channels, while for high values it has larger passages. Besides, Ωs provides maximum achievable efficiency. Analyzing this important parameter, it can be noticed that it can be expressed mathematically through various speed or geometric relationships; the combination of these relationships leads to the definition of a large number of turbines that are different in shape, speed and pressure ratios. The losses listed above are analyzed under the assumption of one-dimensional flow for all geometric configurations. Moreover, the degree of reaction of the turbine is considered constant, while the absolute velocity in the output section is completely axial. The independent variables considered by Rohlik are:

a. Absolute velocity angle at impeller Inlet ($\alpha_1$).
b. Impeller inlet height to mid-span impeller diameter at outlet ratio ($b_1/D_{2mid}$).
c. Mid-span impeller diameter at the outlet to inlet impeller diameter ratio ($D_{2mid}/D_1$).

The results of this study show that, for each specific speed value, maximum efficiency is reached for a particular combination of geometric characteristics and speed ratios. In the technical literature are available various theoretical studies tending to establish the "optimal" geometry and flow parameters of a radial turbine for an assigned characteristic parameter; such optimization studies are based on a one-dimensional flow model and the calculation of the energy loss with correlations, obtained from experimental tests of real machines. The "general" indications provided by them are following experience, those "specific" (such as the values of the efficiency obtained as characteristic parameter function) should be considered as indicative, because of the simplifications that have been adopted in the calculation. Rohlik has calculated the losses and efficiencies of a large number of radial

turbines, belonging to 8 types of machines, characterized by having the impeller inlet angle constant, as project condition. For each impeller and inlet angle (and for every machine configuration) varying the different geometrical ratios ($D_{2mid}/D_1$, $b_2/D_{2mid}$, $b_1/D_1$) and the exit angle $\beta_{2mid,}$ it is possible to design different machines with different characteristic parameters; Rohlik has calculated the internal efficiency for each machine, taking into account the following energy losses:

1. Leaks in the fluid nozzles.
2. Losses fluid into the impeller.
3. Losses due to the "gap" between impeller and case.
4. The loss for ventilation of the rear face of the disk of the impeller.
5. Loss of kinetic energy at the exhaust.

In Figures 8 and 9 are shown and quantified these losses in the function of the characteristic parameter (specific speed, $\Omega_s$). The main constraints in the analysis are:

1. The outlet angle $\beta_2$ on the average diameter $D_{2mid}$ is always chosen to obtain $\alpha_2 = 90°$ (axial discharge);
2. The speed $W_{2mid}$ at mid-span ($D_{2mid}$) has been set to two times the inlet velocity $W_1$ to always have a sufficient reaction degree; the energy losses of an impeller are lower (according to common experience) when the reaction degree is high;
3. To avoid large curvatures of the flow lines of the impeller in the proximity of the casing, it is assumed that $D_{2e}$ is at most equal to 0.7 $D_1$;
4. To limit the effect of excessive value of the blockage factor of the blades, the diameter $D_{2i}$ has to be equal or greater than 0.4 $D_{2e}$;
5. It is assumed that the blades are radial and the flow angle $\beta_1$ is 90°; under these conditions, the flow entry is not "optimal" since losses produced by "shock" are different from zero.

The trend of the efficiency $\eta_t$ for such turbines devices (characterized by a certain angle $\alpha_1^c$), as a function of Ωs, is shown in Figure 8. For a given value of $\alpha_1{}^c$, the architecture of the machine can still vary, and in correspondence, it is possible to obtain different values $\Omega_s$ of the efficiency for each "family" with $\alpha_1{}^c$ = *constant*, within the dashed curve represented in Figure 10. The specific speed (Ωs) is expressed as a function of the characteristic geometric and kinematic parameters, according to Rohlik formulation,in analogy with the current practice in the field of hydraulic turbines, Rohlik introduces the relationship between the speed $U_1$ and the "spouting velocity ($C_{sp}$)":

$$C_{sp} = \sqrt{2 \cdot \left(h_0^0 - h_{2s}^0\right)} \tag{1}$$

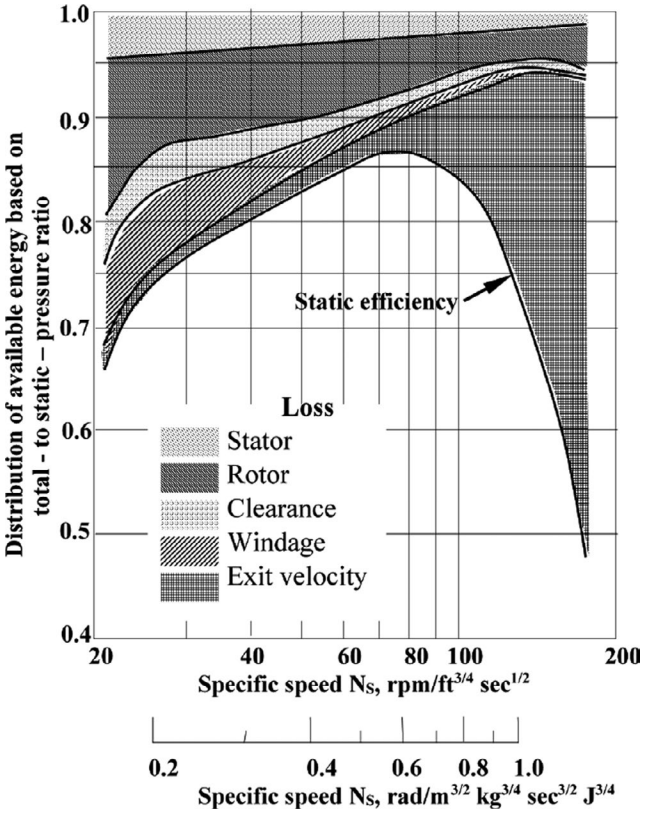


**FIGURE 8** Distribution of losses along envelope of maximum Total-to-Static (adapted from Rohlik)

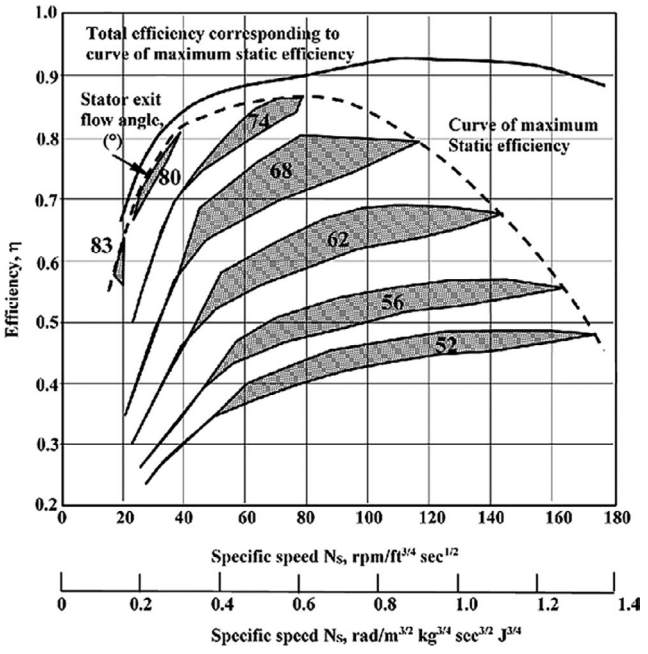


**FIGURE 9** Calculated Performance of 90° IFR Turbine (adapted from Rohlik)

With this definition and the limitations previously imposed, it is possible to compute the specific speed (Ωs) as:

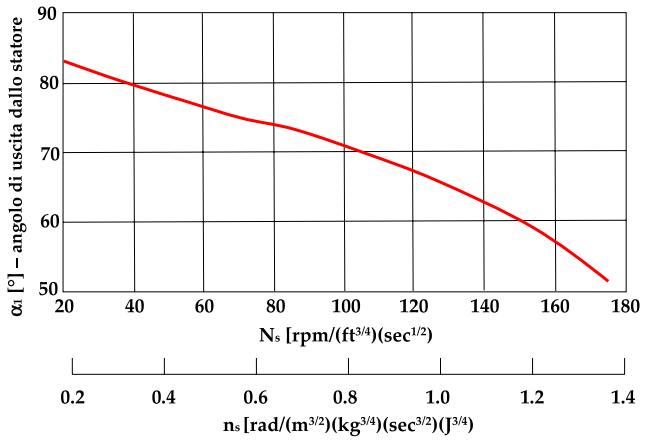


**FIGURE 10** Variation of the impeller inlet angle of the absolute speed corresponding to the maximum efficiency as a function of the specific speed (adapted from Rohlik)

$$\Omega s = (2)^{\frac{7}{2}} \cdot (\pi)^{\frac{1}{2}} \cdot \left( \frac{4 \cdot (\tan \alpha_1^c)^2}{\left(\frac{D_{2\text{mid}}}{D_1}\right)^2} - 1 \right)^{\frac{1}{4}} \cdot \left( \frac{b_2}{D_{2\text{mid}}} \right)^{\frac{1}{2}} \cdot \left( \frac{D_{2\text{mid}}}{D_1} \right)^{\frac{3}{2}} \cdot \left( \frac{U_1}{C_{\text{sp}}} \right)^{\frac{3}{2}} \tag{2}$$

This equation shows that, for a given $\alpha_1^c$, the same value of Ωs can be obtained with different pairs of $D_{2\text{mid}}/D_1$ and $b_2/D_{2\text{mid}}$; from such pairs of values depend (Figures 10 and 11), as can be shown, the geometry of the turbine, the ratio $U_1/C_{\text{sp}}$, and the efficiency $\eta_t$. The work of Rohlik, aimed to obtain maximum efficiency from each family of turbines analyzed and tested, has resulted in a variety of graphs, which, from some design parameters, allow obtaining a valuable guide for the configuration of the impeller. In Figure 9, it is possible, for example, to estimate the angle $\alpha_1^c$ of speed $C_1$ at rotor inlet as a function of the specific speed Ωs. In Figure 11, it is possible to estimate the value of the $U_1/C_{\text{sp}}$ ratio in function of the characteristic parameter Ωs of the machine (in this graph the relationship $U_1/C_{\text{sp}}$ is defined as "blade–jet speed"). A further important result is shown in Figures 12 and 13: the relationship between shroud diameter at the outlet section and diameter at the inlet section of the impeller (or $D_{2e}/D_1$ ratio). There is a physical limit that, once achieved, cannot be exceeded and this limit is due to the fluid that cannot fulfill deflections, so significant, with acceptable efficiency.[2,8,9]

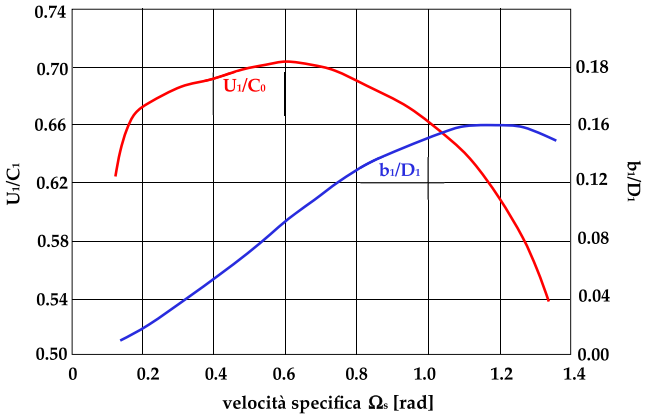


**FIGURE 11** Variation in blade speed spouting velocity ($u_1/c_0$) and nozzle to blade height-rotor inlet diameter ($b_1/d_1$) corresponding to maximum total-to-static

## 2.1 | Design procedure and initial assumptions

To begin our design the first thing to do is to establish the initial parameters that are the base of our design:

$\alpha_1^c$ is taken as the optimal value determined by ROHLIK:

$$\alpha_1^c = 74° \rightarrow \alpha_1 = 90 - \alpha_1^c = 16° \tag{3}$$

From ROHLIK's studies, the following conditions must be respected:

$$\frac{D_{2\text{hub}}}{D_{2\text{shroud}}} \geq 0.4; \quad \frac{D_{2\text{shroud}}}{D_1} \leq 0.7 \tag{4}$$

Then, the mean diameter at the outlet section is:

$$\frac{D_{2\text{shroud}} + D_{2\text{hub}}}{2} = D_{2\text{mid}} \tag{5}$$

In Figure 11 the state "0" is on the stator inlet. Then the states "1" and "2" are on inlet and outlet of the rotor. It can be written that:

$$\frac{D_{2\text{shroud}}}{D_{2\text{mid}}} + \frac{D_{2\text{hub}}}{D_{2\text{mid}}} \tag{6}$$

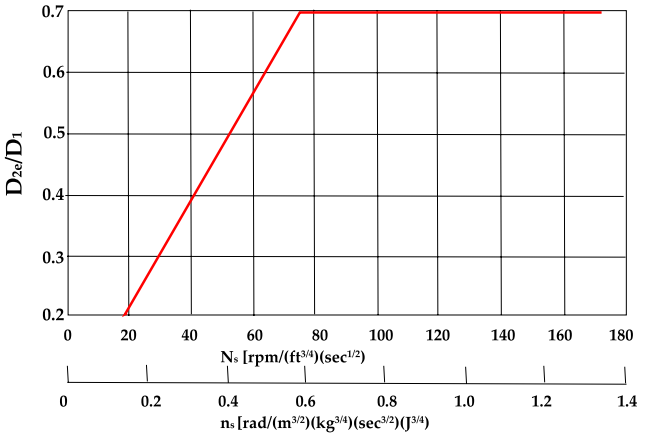


**FIGURE 12** Trend of the ratio between the outer diameter of the outlet section of the impeller and the inlet diameter in function of the index characteristic (adapted from Rohlik)

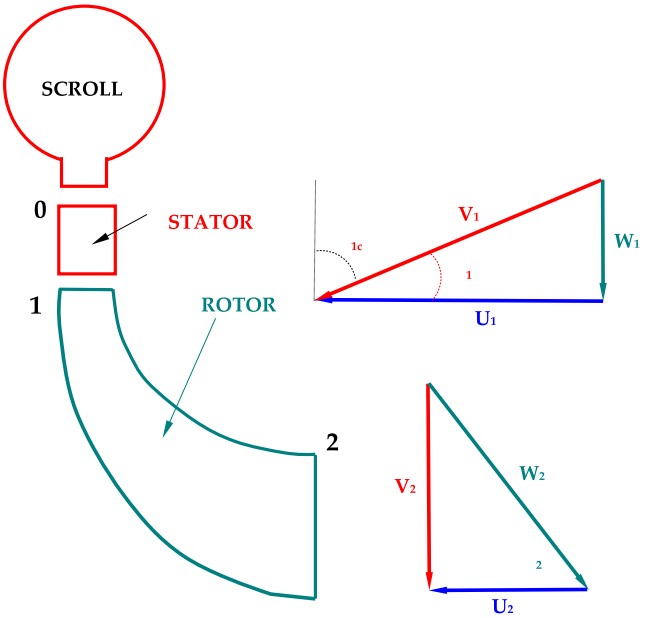


**FIGURE 13** Turbine general scheme and inlet/outlet triangles

$$\frac{D_{2\text{shroud}}}{D_1}\cdot\frac{D_1}{D_{2\text{mid}}}+\frac{D_{2\text{hub}}}{D_{2\text{shroud}}}\cdot\frac{D_{2\text{shroud}}}{D_1}\cdot\frac{D_1}{D_{2\text{mid}}} \tag{7}$$

Substituting values into the equation above, the value of the mid-span diameter at the outlet to inlet diameter ratio is determined:

$$\frac{D_{2\text{mid}}}{D_1} \tag{8}$$

Inlet beta angle equal to 90° (for material resistance reasons): $\beta_1 = 90° \rightarrow \psi_1 = 1$.

Outlet alpha angle equal to 90° (axial flow at the outlet) for every outlet section (mid-span, hub, and shroud).

$$\alpha_2 = 90° \rightarrow \psi_2 = 0$$

Outlet relative velocity at mid-span ($W_{2\text{mid}}$), is twice the relative velocity at the inlet ($W_1$).

$$W_{2\text{mid}} = 2 \cdot W_1 \tag{9}$$

Blade blockage coefficient:

$$\delta_{1-2} = 0.85 \tag{10}$$

## 2.2 | Rotor step-by-step calculation

First of all, it is important to calculate the "spouting velocity":

$$\frac{1}{2}C_{\text{sp}}^2 = h_0^0 - h_{2s}^0 \rightarrow C_{sp} = \sqrt{2\cdot\left(h_0^0 - h_{2s}^0\right)} \tag{11}$$

Then "$\nu$" is calculated as:

$$\nu = \frac{U_2}{C_{\text{sp}}} \tag{12}$$

According to,[2] "$\nu$" must be close to 0.7 for optimal efficiency.

With the available thermodynamic data, the flow rate can be computed, as well as the pressure ratio:

$$Q_0 = \frac{\dot{m}}{\rho_0};\quad Q_2 = \frac{\dot{m}}{\rho_2};\quad \beta = \frac{P_0}{P_2} \tag{13}$$

From the initial assumptions, the reaction degree is:

$$R_\rho = 1 - \frac{\psi_1 + \psi_2}{2} = 0.5 \tag{14}$$

It is possible to calculate $T_1$ and $P_1$:

$$T_1 = T_0 - R_\rho\left(T_0 - T_2\right) \tag{15}$$

$$p_1 = p_0 \cdot \left(\frac{T_1}{T_0}\right)^{\frac{\kappa}{(\kappa-1)\cdot\eta p}} \tag{16}$$

The fluid density on state "1" ($\rho_1$) is derived and then $Q_1$ is computed:

$$Q_1 = \frac{\dot{m}}{\rho_1} \tag{17}$$

Remembering the Euler's work equation and assuming zero the dynamic enthalpy (as an initial approach):

$$h_i^0 = h_i + \frac{v_i^2}{2} \tag{18}$$

$$L_{\text{Eul}} = h_0^0 - h_2^0 \rightarrow \quad \text{with} \quad \frac{v_i^2}{2} = 0 \rightarrow L_{\text{Eul}} = h_0 - h_2 \tag{19}$$

And if:

$$V_{2t} = 0 \rightarrow \psi_2 = 0 \tag{20}$$

It is possible to calculate blade speed $U_1$ as:

$$h_0 - h_2 = U_1^2 \cdot \psi_1 \rightarrow U_1 = \sqrt{\frac{h_0 - h_2}{\psi_1}}. \tag{21}$$

Inlet impeller diameter is so calculated:

$$U_1 = \frac{D_1}{2}\cdot\omega \rightarrow D_1 = \frac{2\cdot U_1}{\omega} \tag{22}$$

Then

$$V_1 = \frac{U_1}{\cos\alpha_1} \tag{23}$$

$$W_1 = U_1 \cdot \sin\alpha_1 \tag{24}$$

From triangle geometry:

$$V_{1t} = U_1;\ V_{1m} = W_1 \tag{25}$$

Blade height can be computed as:

$$b_1 = \frac{Q_1}{\pi \cdot V_{m1} \cdot D_1 \cdot \delta_{1-2}} \tag{26}$$

And the flow coefficient $\Phi_1$:

$$\phi_1 = \frac{V_{m1}}{U_1} \tag{27}$$

For state 2, it is possible to determinate the medium diameter:

$$D_{2\text{mid}} = \frac{D_{2\text{mid}}}{D_1} \cdot D_1 \tag{28}$$

then:

$$U_{2\text{mid}} = \frac{D_{2\text{mid}}}{2} \cdot \omega \tag{29}$$

Remembering that $W_{2\text{mid}} = 2 \cdot W_1$ and from velocity triangle:

$$\beta_{2\text{mid}} = \arccos\frac{U_{2\text{mid}}}{W_{2\text{mid}}} \tag{30}$$

By considering that:

$$V_{2\text{mid}} = V_{m\ 2\text{mid}} = W_{2\text{mid}} \cdot \sin\beta_{2\text{mid}} \tag{31}$$

the flow coefficient at mid-span is:

$$\phi_{2\text{mid}} = \frac{V_{m\ 2\text{mid}}}{U_{2\text{mid}}} \tag{32}$$

It is possible to calculate the blade height at the outlet section:

$$b_2 = \frac{Q_2}{\pi \cdot V_{m\ 2\text{mid}} \cdot D_{2\text{mid}} \cdot \delta_{1-2}} \tag{33}$$

The shroud and hub diameter are given by:

$$D_{2\text{shroud}} = D_{2\text{mid}} + b_2; \quad D_{2\text{hub}} = D_{2\text{mid}} - b_2 \tag{34}$$

Blade speeds at different diameters are calculated:

$$U_{2\text{shroud}} = \frac{D_{2\text{shroud}}}{2} \cdot \omega; \quad U_{2\text{hub}} = \frac{D_{2\text{hub}}}{2} \cdot \omega \tag{35}$$

And then:

$$\phi_{2\text{hub}} = \phi_{2\text{mid}} \cdot \frac{D_{2\text{mid}}}{D_{2\text{hub}}}; \quad \phi_{2\text{shroud}} = \phi_{2\text{hub}} \cdot \frac{D_{2\text{hub}}}{D_{2\text{shroud}}} \tag{36}$$

from this:

$$\beta_{2\text{shroud}} = \tan^{-1}\phi_{2\text{shroud}}; \quad \beta_{2\text{hub}} = \tan^{-1}\phi_{2\text{hub}} \tag{37}$$

Finally:

$$W_{2\text{hub}} = \frac{U_{2\text{hub}}}{\cos\beta_{2\text{hub}}}; \quad W_{2\text{shroud}} = \frac{U_{2\text{shroud}}}{\cos\beta_{2\text{shroud}}} \tag{38}$$

$$V_{2\text{hub}} = V_{m\ 2\text{hub}} = W_{2\text{hub}} \cdot \sin\beta_{2\text{hub}} \tag{39}$$

$$V_{2\text{shroud}} = V_{m\ 2\text{shroud}} = W_{2\text{shroud}} \cdot \sin\beta_{2\text{shroud}} \tag{40}$$

The last step is to verify that:

$$\frac{D_{2\text{hub}}}{D_{2\text{shroud}}} \geq 0.4; \quad \frac{D_{2\text{shroud}}}{D_1} \leq 0.7 \tag{41}$$

To obtain the indicative value of efficiency of the turbine, considering the different losses estimated by ROHLIK, the specific speed $\Omega_s$ is calculated with the equation proposed by Dixon:[8]

$$\Omega_s = 2,11 \cdot \left(\frac{c_2}{c_0}\right)^{1/2} \cdot \left(\frac{A_2}{A_d}\right)^{1/2} \tag{42}$$

where $c_0$ is the spouting velocity and:

$$A_2 = \frac{Q_2}{V_2}; \quad A_d = \frac{\pi \cdot D_1^{1/2}}{4} \tag{43}$$

To initiate another iteration, the new "grades of reaction" are calculated as:

$$R_{\rho\text{mid}} = 1 - \frac{\psi_1 + \psi_2}{2} + \frac{\phi_1^2 - \phi_{2\text{mid}}^2}{2 \cdot (\psi_1 - \psi_2)} \tag{44}$$

$$R_{\rho\text{hub}} = 1 - \frac{\psi_1 + \psi_2}{2} + \frac{\phi_1^2 - \phi_{2\text{hub}}^2}{2 \cdot (\psi_1 - \psi_2)} \tag{45}$$

$$R_{\rho\text{shroud}} = 1 - \frac{\psi_1 + \psi_2}{2} + \frac{\phi_1^2 - \phi_{2\text{shroud}}^2}{2 \cdot (\psi_1 - \psi_2)} \tag{46}$$

Once again, taking as initial parameter $R_{\rho,\text{mid}}$, another iteration starts, with the same sequence of calculation described above. When the iterations are convergent, it proceeds to calculate the number of blades for the impeller. There are two different approaches, to compute this parameter.[2,9]

## 2.3 | The conservative approach

$$Z_{\text{rot}} \geq 2 \cdot \pi \cdot \cot\alpha_1 \tag{47}$$

With $\alpha_1$ in radians. This formula supplies a blades number that, sometimes, can be excessive. Depending on the general dimensions of the turbine.

## 2.4 | A less restrictive approach

$$Z_{\text{rot}} \geq \frac{\pi}{30} \cdot \left(\alpha_1^{\circ} + 20\right) \cdot \cot\alpha_1 \tag{48}$$

where $\alpha_1^{\circ}$ is the angle in degrees and $\alpha_1$ is the angle in radians. The next step is to determine the geometry of the stator or nozzles.

### 2.4.1 | Nozzle step-by-step calculation

The initial assumptions are:

$$b_0 = b_1$$

$$\alpha_{1\text{sta}} = \alpha_1$$

$$\frac{D_0}{D_{1\text{sta}}} = 1.3$$

$$\delta_{0-1} = 0.85$$

Leaving some space between nozzle final section and rotor leading edge, the outlet diameter of the stator (state "$1_{\text{sta}}$") can be calculated as:

$$D_{1\text{sta}} = D_1 + 0.004 \quad (m) \tag{49}$$

the diameter at state 0 is computed:

$$D_0 = 1.3 \cdot D_{1\text{sta}} \tag{50}$$

The number of blades is often calculated with the formula:

$$Z_{sta} \approx Z_{rot} - 2 \tag{51}$$

From:

$$\frac{P_0}{\rho_0} - \frac{P_1}{\rho_1} = \frac{V_{1m}^2}{2} \cdot \left[\left(1 + \frac{1}{\left(\tan\alpha_{1\text{sta}}\right)^2}\right) - \frac{\rho_1}{\rho_0}\left(\frac{b_{1\text{sta}} r_{1\text{sta}}}{b_0 r_0}\right)^2 \left(1 + \frac{1}{\left(\tan\alpha_0\right)^2}\right)\right] \tag{52}$$

the value of $\alpha_0$ can be calculated with the formula:

$$V_{0m} = \frac{\rho_1 \cdot V_{1m} \cdot r_{1\text{sta}} \cdot b_{1\text{sta}} \cdot \delta_{0-1}}{\rho_0 \cdot r_0 \cdot b_0 \cdot \delta_{0-1}} \tag{53}$$

Then, $V_{0t}$ is:

$$V_{0t} = \frac{V_{0m}}{\tan\alpha_0} \tag{54}$$

The procedure has been studied to make all machinery design independent of the fluid, using only thermodynamic data. Finally, the flow chart of the design procedure is represented in Figure 14.

# 3 | SCREW EXPANDERS DESIGN PROCEDURE

The design of screw expanders consists of two rotors (male and female screws) connected to the corresponding counter-rotating shafts, that transmit the motion to an electric generator. The fluid is expanded in the axial direction, in the volume that is generated between the lobes of the screws. The fluid fills the volume between the screws isolated and then downloaded into the area of low-pressure discharge.

## 3.1 | Rotor profiles

The rotor profile is the fundamental feature of such machinery. The earliest machines used asymmetric profiles, as shown in Figure 15. It can see that the male rotor is built by only three circles, which are located in the center and on the pitch circle. The profile of the female rotor is symmetrical to this construction. The symmetric profile has a very large blow-hole area which creates significant internal leakage. This negative feature excludes the use of this machine in all these systems that have a high and moderate pressure ratio. Following the introduction of the symmetrical circular profile, many improved profiles have been developed and studied. Among these, the "N" profile, developed at City University, has many advantages than any other device. Currently, it is the most used profile by the various manufacturers. One of the advantages is the high adiabatic efficiency, even for low operating speeds. The benefits of

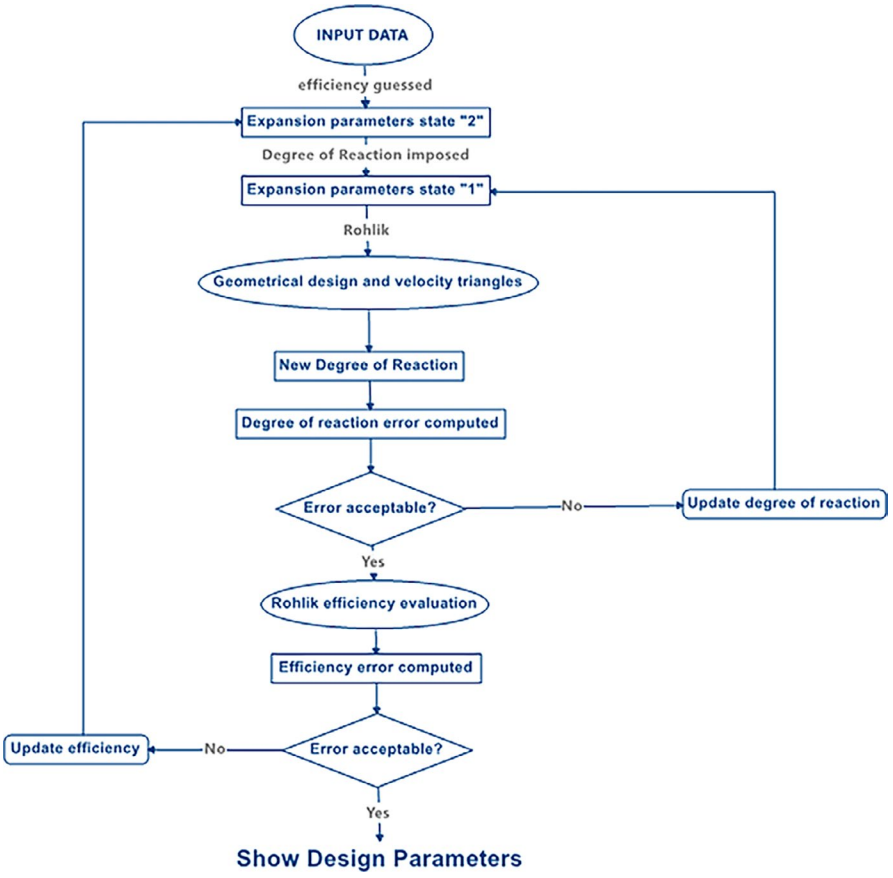


**FIGURE 14** Flow chart of IFR design procedure

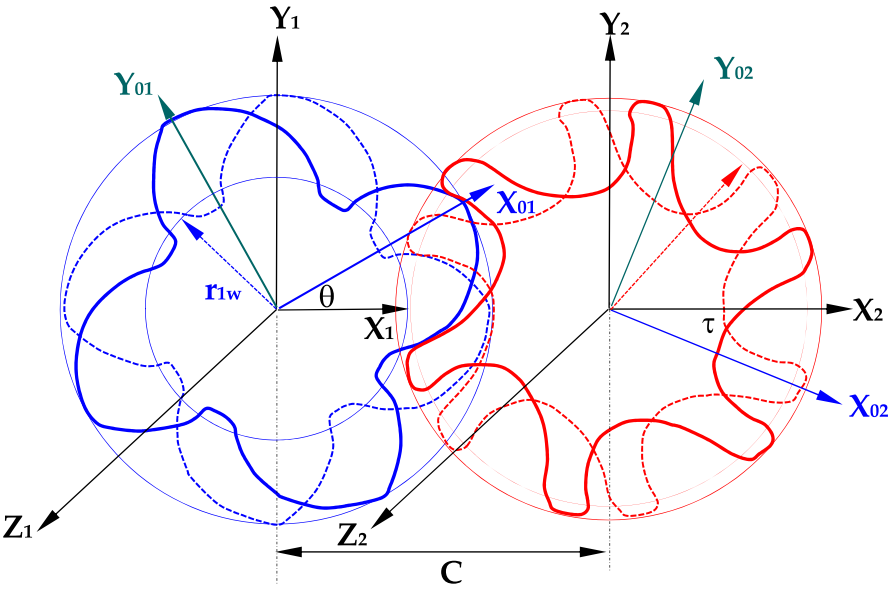


**FIGURE 15** Symmetric circular profile

more than 10% were recorded compared to other profiles. A typical pair of rotor profiles "N"[10,11] is shown in Figure 16.

## 3.2 | Screw expanders characteristics

The screw expanders can process both gas (air) and steam; as for the steam, they can process overheated, humid or saturated one, with a mixture ratio lower than one. These machines allow the chosen working fluid to expand from an inlet pressure $p_{in}$ to the exhaust flange pressure $p_{out}$. This pressure difference is the only requirement needed to have a functioning machine. The fluid is elaborated thanks to the two above mentioned screws (male screw and female screw) that, with the casing, define the working volume; one of these two screws is coupled directly to a generator or, at most, to a mechanical variable-speed drive. The screws, initially, had a symmetrical profile with an equal number of lobes; however, with the implementation of

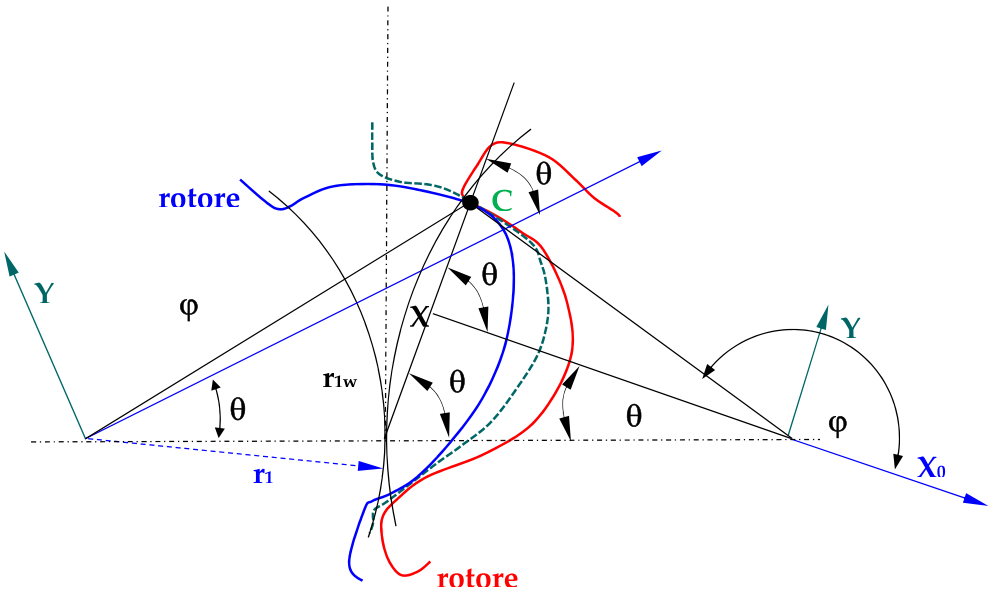


**FIGURE 16** Rack generated "N" Profile (London City University)

computational fluid dynamics programs, it has opted for an asymmetrical profile and with a different number of lobes, between male and female (4-6 or 5-6). Newer machines have adopted a profile defined in "N", developed at the City University of London. This profile also has other advantages, including lower transmission torque (with a relative decrease of friction), strong female rotors, a dedicated large processing volume for the fluid, and a shorter seal between the rotors, which guarantees a loss reduction, due to leakage. This profile is now well-proven and used by many leading companies in the world of screw machines. Overall, using this profile allows increasing the machinery adiabatic efficiency, especially with the apex speed of the rotor, lower compared to traditional profiles. The efficiency gain has been experimentally confirmed by about 10%. The most significant advantages of profile "N" are as follows:

1. Ensures that, at each point of contact, a hermetic seal between the rotors and between the rotors and the seat is realized, in such a way as to prevent leakage of working fluid during operation.
2. It provides a large area of passage through the lobes, which maximizes the amount of fluid for each revolution.
3. The coupling movement is the same as a helicoid pair with low contact force intensity.

This allows the machine to work without tools that monitor the valve timing, and reduces internal frictions, reducing its mechanical inefficiencies. Finally, a key feature of the screw expander, adopting "N" the profile, lies in the fact that the fluid speed is about an order of magnitude lower than turbomachines ones, furthermore there is no damage risk, caused by the entry of liquid particles in the expansion chamber, as the propeller profile is continuous, and therefore, there are no problems of droplet impact on profiles. In this way, these expanders may accept a steam flow rate, with any mixture ratio, from saturated liquid to dry steam. The condensate also has a positive effect on the efficiency of the machine, because it performs such a sealing, decreasing leakage losses. As regards realization, the single screw, it is fully generated using machine tools, ensuring extremely high structural reliability. Moreover, considering also the production simplicity and wide dissemination of screw machinery, the technological process ensures a low cost of implementation. Today the production of propellers for screw expanders ensures a low cost if the diameter of the rotor (screw) is less than or equal to 350–400 mm. These machines can rotate at high speeds compatible with main grid frequency, but thanks to the small diameter, the rotor tip speed is generally an order of magnitude lower than traditional turbines; this translates into the ability to connect directly to the alternator rotor, reducing costs (lack of a mechanical gearbox), increasing the reliability and increasing the overall machine efficiency. Considering as a reference several of studies,[11,12] it was found that for a power range between 20 and 50 kW and a rotation speed of between 1,500 and 1,800 rpm, the tip speed ranges between 8 and 15 m/s.

## 3.3 | Thermodynamic analysis

Screw expanders allow the working fluid to expand in volume bounded by screw lobes. The thermodynamic cycle of an ideal expander (P–V chart, Figure 17) is characterized by:

1. Working fluid admission pressure constant;

2. Fluid isentropic expansion with an initial specific volume $v_{inlet}$
3. A discharge pressure of working fluid exhausted constantly

The ratio $\beta$ is defined as the relationship between the expander inlet pressure ($p_{inlet}$) and exhaust pressure ($p_{outlet}$). Similarly, $\beta_\varepsilon$ as the pressure ratio at the beginning of the expansion ($p_{exp}$) and the pressure at the end ($p_{ex}$) of the process itself. In the case of ideal expansion, these two ratios are to be the same. However if $\beta_\varepsilon - \beta > 0$ a "blow-down" phenomenon (Figure 17b) is established, while $\beta_\varepsilon - \beta < 0$ the "blow-back" occurs (Figure 17c). In Figure 17, the expansion of a screw expander is reported:

1. An ideal expansion with no leakage and where the expander outlet pressure is equal to the discharge pressure;
2. An expansion into Blow-Down condition; in this case, the outlet pressure is higher than the discharge pressure. This condition represents the real working condition because for delivering the fluid, a discharge overpressure has to be maintained;
3. An expansion in Blow-Back condition. This is the worst condition for the expander operating mode. In fact, at the expander outlet, compression of the working fluid occurs, because the expander outlet pressure is lower than the discharge one.

The cycles presented are far from the actual configuration. In the real cycle several losses can be listed:

1. Pressure drops during the working fluid admission and discharge;
2. Nonisentropic expansion, due to the passive resistance;
3. Irreversibility losses in blow-down and blow-back phenomena;
4. Leakage losses through the seals.

Considering the P–V diagram in Figure 17, it can be noticed, during the admissions process, that the status of the working

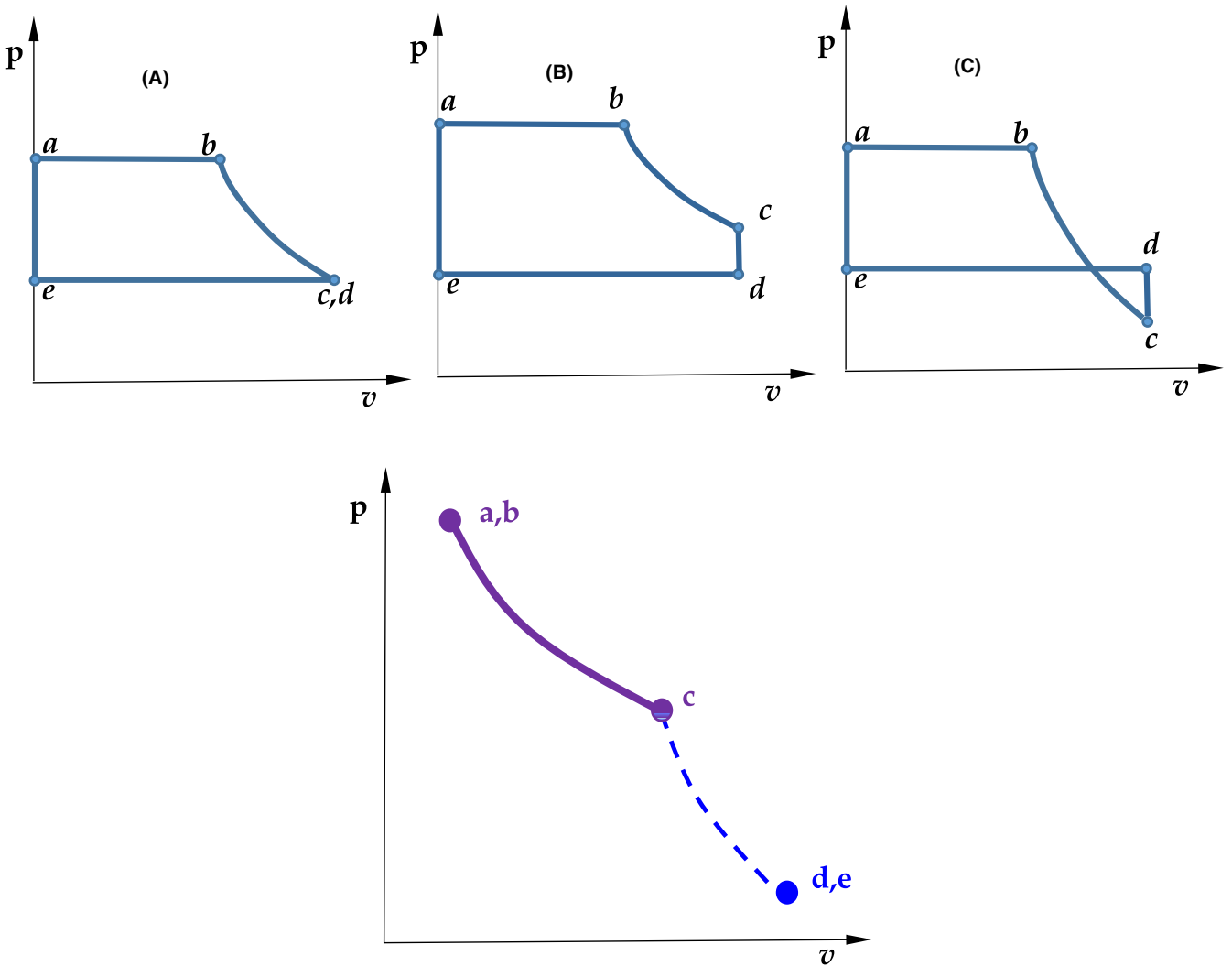


**FIGURE 17** A, Expansion on p-V diagram. B, Details of the expansion process

fluid remains constant (points *a*, *b* and *d*, *e*). The rotor movement, during the expansion process, varies the fluid specific volume by *b* to *c*. However, the Blow-Down process is instantaneous and irreversible and causes power losses compared to the ideal case.[13] Considering the process conditions, the work can be evaluated adding each contribution. This is achieved by imposing the condition such that the volume balance between the *c* and d is constant, because in that section, expansion is instantaneous, and, therefore, there is no variation in volume between these two points of the thermodynamic cycle. For each transformation, the work is calculated, to achieve a final total cycle work definition (Equations 55-61).

$$W_{ab} = -\dot{m}_{in} \cdot \left(u_b - h_b\right) = \dot{m}_{in} \cdot p_b \cdot v_b \tag{55}$$

$$W_{bc} = -\dot{m}_{in} \cdot \left(u_c - u_b\right) = \dot{m}_{in} \cdot \left(h_c - h_b\right) - \dot{m}_{in} \cdot \left(p_b \cdot v_b - p_c \cdot v_c\right) \tag{56}$$

$$W_{cd} = 0 \tag{57}$$

$$W_{de} = -\dot{m}_{\text{out}} \cdot \left(u_d - h_d\right) = \dot{m}_{\text{out}} \cdot p_d \cdot v_d \tag{58}$$

So:

$$W_{\text{tot}} = W_{ab} + W_{bc} + W_{cd} + W_{de} \tag{59}$$

Then:

$$\dot{m}_{\text{in}} v_c = \dot{m}_{\text{out}} v_d \tag{60}$$

$$k = \left(\frac{h_c}{h_c + h_d}\right) - \left(\frac{v_c \cdot \left(p_c - p_d\right)}{h_c + h_d}\right) \tag{61}$$

Finally:

$$W_{\text{tot}} = \dot{m}_{in} \cdot \left[h_b - \left(\frac{k}{1-k}\right) \cdot h_d\right] + \dot{m}_{in} v_c \cdot \left(p_c - p_d\right) \tag{62}$$

Once the theoretical work has been computed, it is possible to define the actual machine work, evaluating the available shaft power with Equation (62). It is easier to assess these parameters compared to evaluate the real conditions of working fluid at the end of the expansion, due to the multiphase nature of the process.

$$W_{\text{real}} = N \cdot \omega \tag{63}$$

The total efficiency is given by:

$$\eta_{\text{tot}} = \eta_t \cdot \eta_d \cdot \eta_{\text{mech}} \tag{64}$$

From Equations (64) and (65) it is possible to evaluate the different system efficiency.

1. $\eta_t = \eta_\tau(\beta, \beta_\varepsilon)$ This efficiency identifies the power loss, resulting from the unbalance between the admission and discharge pressure compared to actual operating conditions. This condition depends on the concentrated and distributed pressure drop along with the device piping/manifold system. It also depends on the actual operating conditions of the device itself. As previously described, for reliability reasons, the expander usually operates in a Blow-Down condition.
2. $\eta_d$ This efficiency expresses, in a single parameter, the volumetric and isentropic efficiency and it can be evaluated through the direct operating parameters measurement and mechanical losses estimation.
3. $\eta_s$ It is the isentropic efficiency and depends on the thermodynamic transformation, and is an intrinsic property of screw Expander.
4. $\eta_v = m_{\text{out}}/m_{\text{in}}$ It is the volumetric efficiency, due to the leakage losses, which decrease the effective machine flow rate.
5. $\eta_{\text{mech}}$ It is the mechanical efficiency and is due to friction in the machine.

## 3.4 | Losses

In a screw expander, two different losses affect the machine performance, divided into leakage losses and fluid dynamic losses. Leakage losses are linked to the clearances between the various rotor moving parts and the case. These cannot be eliminated since they are intended to ensure an expansion gap of moving parts, subjected to thermal and mechanical stress. Several losses can be identified:

- The rotors line of contact
- The vent formed between the rotors cusps and point of contact
- Losses on top of the rotors
- Losses on the inlet surface of the rotors
- Losses on the outlet surface of the rotors

During the expansion, leakage losses mean that the volumetric efficiency decrease due to the decrease of the processed flow rate (Figure 18a,b). Observing the operating conditions, the losses diminish, if the mixture ratio of the working fluid decreases. The formed liquid acts as a

$$\eta_d = \eta_v \cdot \eta_s = \frac{W_{\text{real}} + W_{\text{real}(N)}}{\dot{m}_{\text{in}} \cdot p_{a,\ \text{real}} \cdot v_a \cdot \left[\frac{\left(1-\beta_{bd}^{1-\gamma}\right)}{\gamma - 1} + \left(1 + \frac{\beta_{bd}}{\beta_\varepsilon}\right)\right]} \quad \text{with} \quad \beta_{bd} = \text{pressure ratio at blow-down condition.} \tag{65}$$

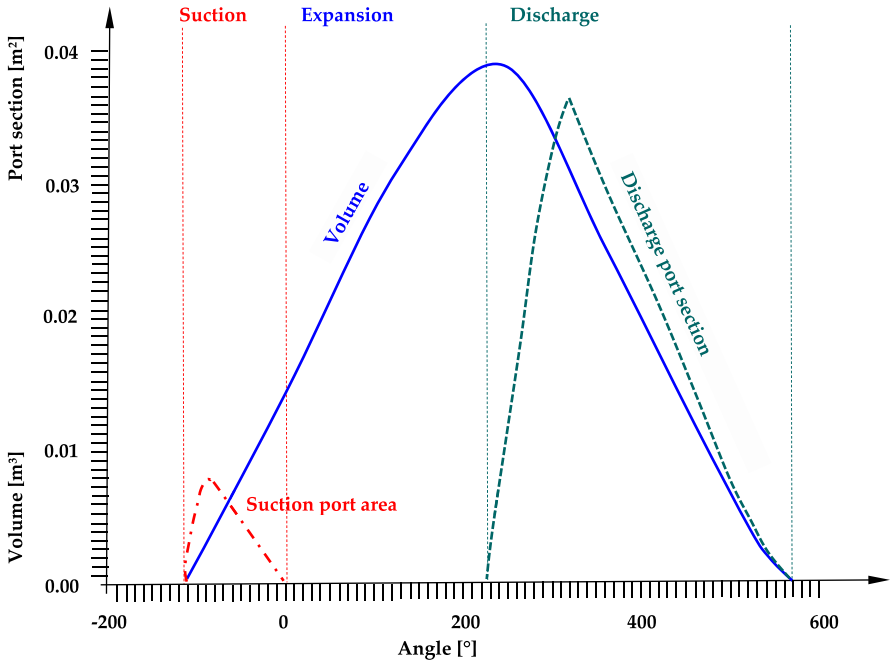


**FIGURE 18** A, Pressure/Chamber volume curve of a screw-type expander (adapted from 10). B, Volume curve of a screw-type expander over the rotational angle of the male rotor (adapted from 10)

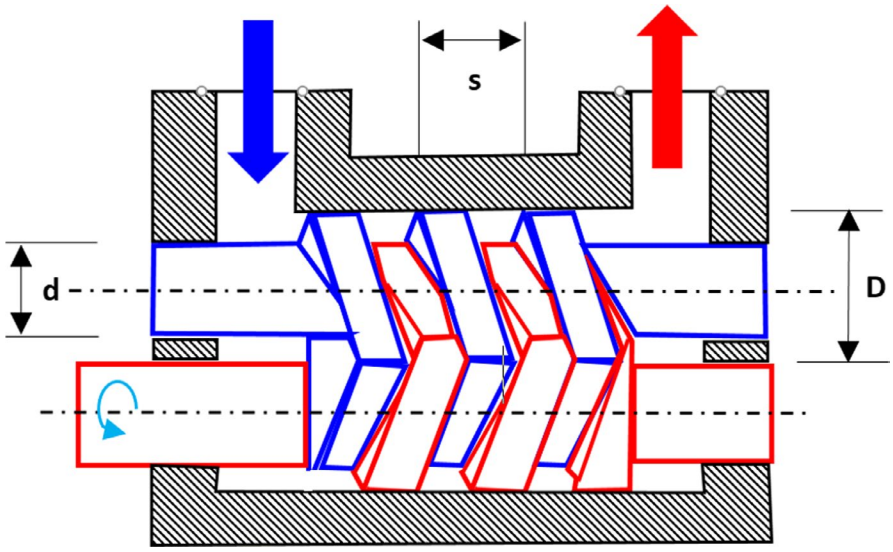


**FIGURE 19** Screw expander geometric characteristics for calculation

sealant between the clearances, and as a lubricating medium, for the moving parts. Considering fluid dynamic losses, some aspects should be considered. In admission, the inlet pressure is not constant. There are concentrated losses due to the interaction between the fluid vein and the profiles (edges) of the various machine ducts. Some researchers have shown that the loss coefficient does not depend on the inlet fluid velocity. However, this loss should not be underestimated, as the working fluid is in a state of humidity. In fact, at the same input speed, the increase in density increases the losses (with the square of the velocity). It can be seen that the expansion is characterized by distributed losses, due to the friction between the working fluid and the wall of the chamber. Finally, it can always opt for a blow-down cycle.

## 3.5 | Displacement calculation

In Figure 19 the reference cross-section to compute the displacement of the machine is presented. So, the displacement can be calculated as

$$V = D^2\left[\frac{\pi}{4}\left(1-d^2\right)-\left(\frac{\alpha}{2}-\frac{\text{sen}2\alpha}{2}\right)\right]\cdot s \quad \text{with } \cos\alpha = \frac{(D+d)}{2D} \quad (\alpha = \text{screw thread inclination}). \tag{66}$$

The elaborated flow rate is a function of the machine rotational speed "n" and the volumetric efficiency "$\eta_v$":

$$Q = \eta_v \cdot D^2 \cdot \left[\frac{\pi}{4}\left(1-d^2\right)-\left(\frac{\alpha}{2}-\frac{\text{sen}2\alpha}{2}\right)\right]\cdot s \cdot n \tag{67}$$

### 3.5.1 | Single Screw displacement calculation

The adopted reference system (z;r) is centered on the crossing point between the main rotor rotational axis and the perpendicular star wheel axis (Figure 20). Generally, the design of a single screw expander relies on the selection of the main rotor diameter $D_{sr}$. It is possible to demonstrate that all the most important dimensions are correlated to the main rotor diameter.[13–16] The swept volume is calculated by correlating the engaging tooth area into the corresponding groove and the tooth engaging angle. Generally, two approaches can be considered to obtain the engaging area, ie through an analytic function or a polygonal approach which requires the definition of four corner points of a tooth at each rotation angle. The engaging angle of each tooth, defined as the angle between the first point of contact of the tooth with one flank of the groove until the tooth completely disengages the groove, is approximately $\alpha_{sw} = 90°$, which corresponds to $\alpha_{sr} \approx 160°$. The maximum groove volume is calculated as a sum of two contributions, $V_o = V_{g,1} + V_{g,2}$, related to geometry-defined angles. The first part represents the volume between suction angle and closing angle and the second part is the volume from the closing angle to the discharge angle. Normally, the maximum groove volume is associated with the discharge volume, ie $V_o = V_2$, which is related to the suction volume $V_1$ using the volumetric built-in ratio, fixed by design. Here follow the list of kinematic and geometry adopted in the calculation.[17,18,19]

The volume of the groove at each star wheel angle (or equivalently main rotor angle) can be calculated by describing the engaging tooth surface with a local reference system ($x$; $y$) on the tooth. The expression of the swept volume is given by splitting the contribution into $V_{g,1}(\theta_{sw})$ and $V_{g,2}(\theta_{sw})$:

$$Vg,1\left(\theta_{sw}\right) = \frac{i}{2}\cdot \int_{\beta_2+\beta^*}^{\theta_{sw}} \int_{-\frac{w}{2}}^{B} \frac{1}{\cos\theta_{sw}} \cdot \left[R_{sr}^2 - \left(d_{sr,sw} - \sqrt{R_{sw}^2 - y^2}\cdot\cos\theta_{sw} + y\,\mathrm{sen}\,\theta_{sw}\right)^2\right] \cdot \mathrm{d}y\mathrm{d}\theta_{sw} \quad \beta_s + \beta^* \le \theta_{sw} \le \beta_{clousre} \tag{68}$$

$$Vg,2\left(\theta_{sw}\right) = V_0 - \frac{i}{2}\cdot \int_{\theta_{sw}}^{\beta_d} \int_{-\frac{w}{2}}^{\frac{w}{2}} \frac{1}{\cos\theta_{sw}} \cdot \left[R_{sr}^2 - \left(d_{sr,sw} - \sqrt{R_{sw}^2 - y^2}\cdot\cos\theta_{sw} + y\,\mathrm{sen}\,\theta_{sw}\right)^2\right] \cdot \mathrm{d}y\mathrm{d}\theta_{sw} \quad \beta_{clousre} < \theta_{sw} \le \beta_d \tag{69}$$

The absence of an analytic solution brings to a numerical calculation of the volume with fixed increments of the rotation angle. A polynomial function is used to interpolate the discrete values and to obtain a continuous function, as well as, to guarantee the continuity of its derivative, necessary to solve the system of differential equations. Finally, by recalling

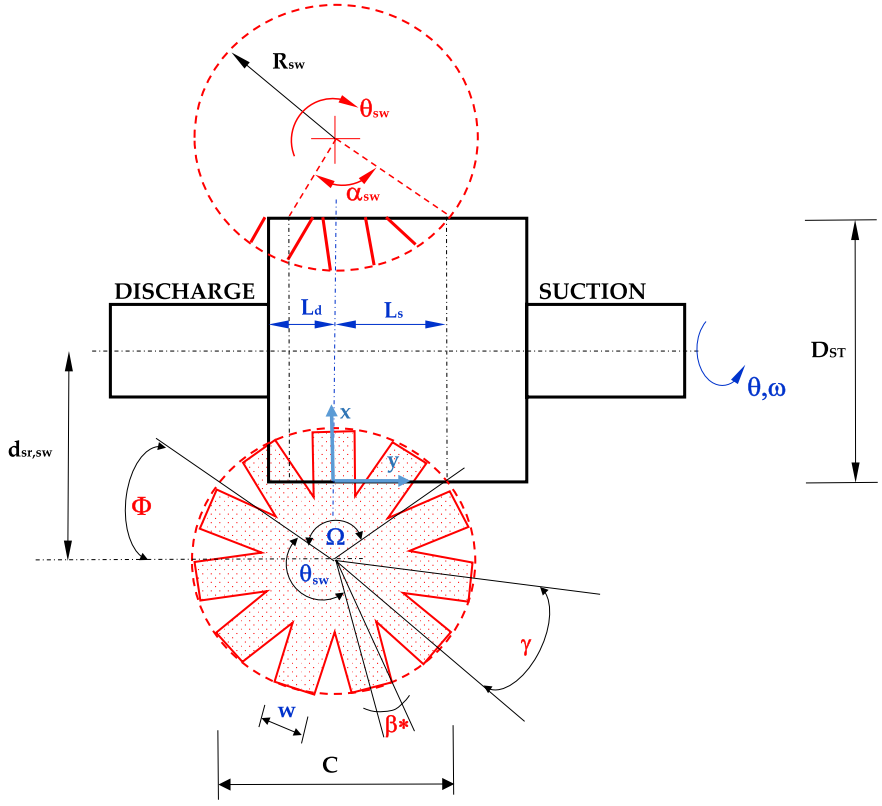


**FIGURE 20** Reference section of a single screw expander for the calculation[15]

that the expansion process occurs symmetrically in both sides of the main rotor, the theoretical volumetric flow rate is so defined:

$$V_{\text{theor}} = 2 \cdot z_{sr} \cdot V_1 \cdot n \tag{70}$$

In Figure 21 is shown the measured efficiency versus pressure and volume ratio and in Figure 22 the flow chart of design procedure.

| Parameter | Value |
|---|---|
| $r_{v,\text{built-in}}$ | $V_2/V_1$ |
| $D_{sr}$ | constant |
| $A_{sw}$ | $½\,\pi\,\alpha_{sr} = ½\,\iota\,\pi$ |
| $R_{sw}$ | $\lambda_d R_{sr}$, $\lambda_d = 1$ to 1.1 |
| $\lambda_{opt}$ | $f(\gamma, \lambda_d)$ |
| $d_{sr,sw}$ | $\alpha_{opt} D_{sr}$ |
| $w$ | $\approx 0.3 R_{sr}$ |
| $\gamma$ | $2\pi/z_{sw}$ |
| $\beta_s$ | arc cos $[(d_{sr,sw} - R_{sr})/R_{sw}]$ |
| $\beta^*$ | arc sen $(w/2\,R_{sw})$ |
| $\beta_d$ | $-\alpha_{sw} - \beta_s - \beta^*)$ |
| $\theta$ | arc sen $[(2d_{sr,sw} - D_{sr})/D_{sw}]$ |
| $\Omega$ | $\pi - 2\theta$ |
| $C$ | $2R_{sw}$ sen$(\Omega/2)$ |
| $L_s$ | $R_{sw}$ sen $\beta_s$ |
| $L_d$ | $R_{sw}$ sen $\beta_d$ |
| $L_{eff}$ | $L_s + L_d$ |

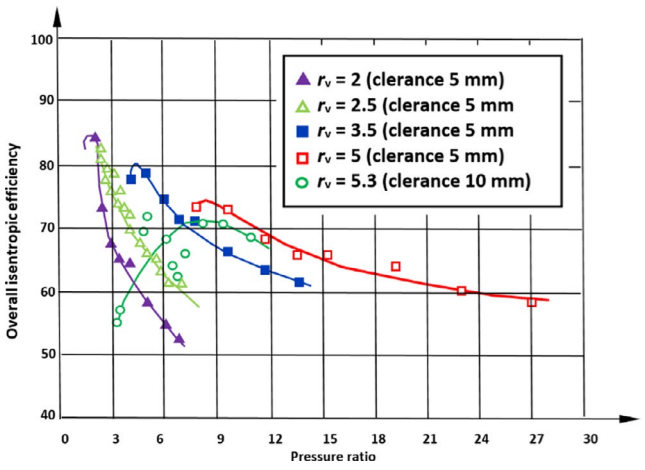


**FIGURE 21** Measured efficiency map in function of pressure and volume ratio [reworked from 10,20]

## 4 | SCROLL EXPANDER DESIGN PROCEDURE AND OPERATING PRINCIPLES

These machines are formed by two spirals positioned reciprocally with central symmetry, one of the two is fixed and the other is movable (Figure 23). Their position defines a series of crescent chambers where the fluid expands, generating the (eccentric) rotation of the movable element on the fixed one. Both components must be manufactured in an optimum way to ensure excellent water tightness and high efficiency of the expander. The working cycle starts with the fluid admission in the chamber that forms at the center of the two spirals. Subsequently, the fluid tends to expand generating the eccentric movement of the movable component and the rotation of the machine crankshaft. While the fluid is still expanding in correspondence with the suction port. At the end of the expansion process, the chamber is unloaded in correspondence to the exit port. This type of expander has a volumetric ratio fixed by the machine geometry and can provide a precise expansion ratio. If the required ratio is different from the intrinsic value of the expander, there are significant losses, which can penalize the efficiency of the machine. The scroll expanders have less noise and longer durability as they do not require suction or discharge valves for their operation. Besides, the particular type of motion offers less resistance than the sliding motion and also acts as a seal, thus making it possible to limit or eliminate the use of lubrication oil. Scroll geometry is so defined, with the following parameters:

1. Orbiting angle.
2. The radius of the basic circle of the scroll.
3. Height of scroll vanes.
4. The initial angle of the outer involute.
5. The initial angle of the inner involute.
6. Starting angle of the outer involute.
7. Starting angle of the inner involute.

The built-in volume ratio is defined as the ratio of the volume of the expansion chamber, at the process end, to the volume of the intake chamber, at the beginning. The built-in volume ratio determines the operating flow rate. It is important to remember that, ideally, the two halves of a scroll remain perfectly in contact, during rotation. Actually, due to the required tolerance, a narrow gap remains. this gap is normally 1 μm wide. If it is increased to 8 μm, the machinery loses its operating characteristics. Two different leakages are considered: radial and axial. Radial leakage is present between adjoining flanks of the vanes. The axial leakage occurs between the vane tip and the base plate of

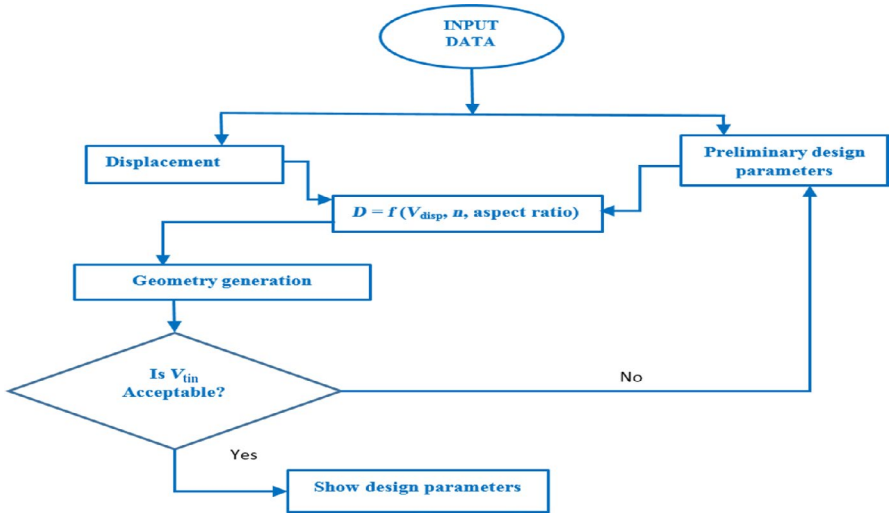


**FIGURE 22** Flow chart of Screw Expander design procedure

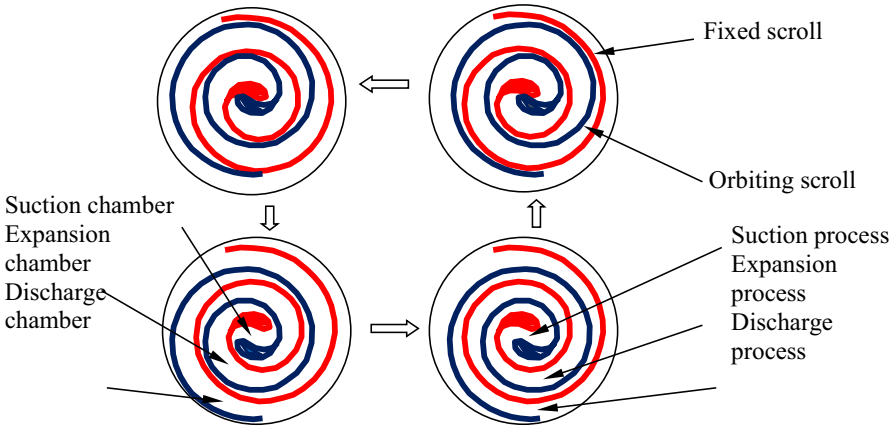


**FIGURE 23** Scroll operating principle

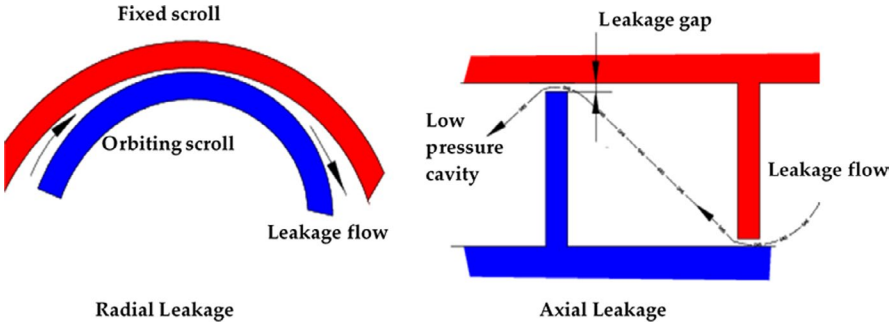


**FIGURE 24** Leakage in a scroll machinery

the opposite scroll (see Figure 24). The direction of the radial leakage is from the high-pressure side towards the low one. This bypass decreases the expander net power. Scroll expanders have numerous advantages, namely:

1. More efficient over their entire operating range.
2. Operate at lower sound and vibration levels than traditional expanders.
3. Fewer moving parts.
4. Ability to start under any system load, without assistance during starting.
5. Easy to service and maintain due to their compact size, lightweight, and simple design.
6. No complex internal suction and discharge valves.
7. Quieter operation and higher reliability due to fewer moving parts.
8. Since high-pressure gas exerts pressure in all directions (tangentially, radial and axially) the requirement for the axial bearing is omitted.

Finally, Figure 25 shows the different scroll position during the operating phases.

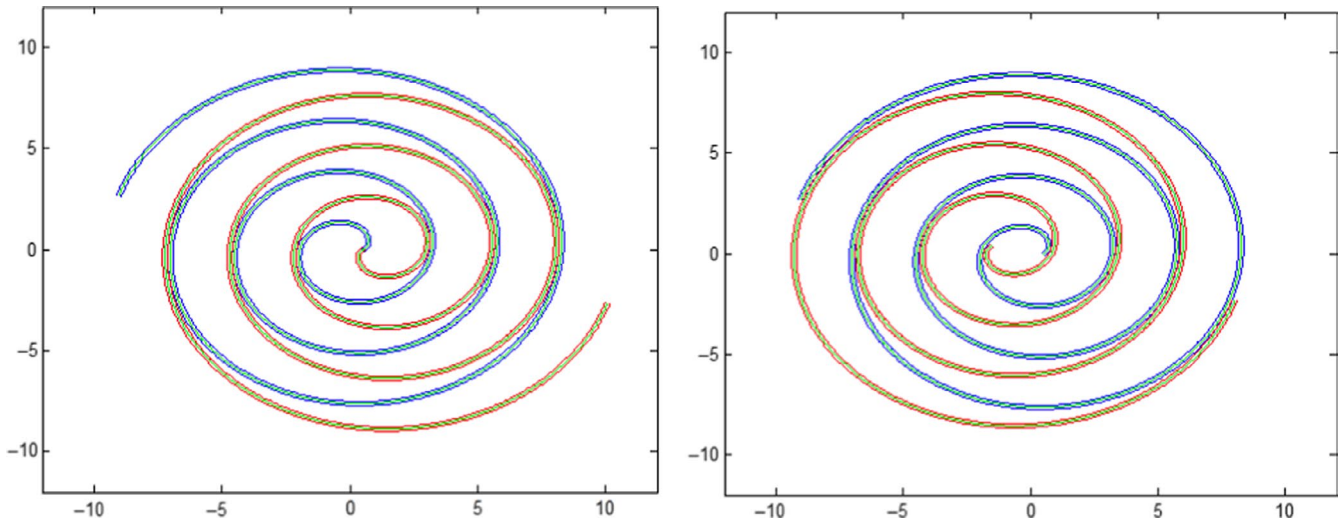

**FIGURE 25** Different scroll position in function of the operating phases

## 4.1 | Energy equation

A pocket is taken as the control volume.[17] The kinetic energy and the potential energy of the fluid flowing in and out of the control volume are neglected. Based on the conservation equation, the following energy balance is obtained:

$$\mathrm{d}(m\cdot u)=\mathrm{d}Q+\sum \mathrm{d}m_{\mathrm{in}}\cdot h_{\mathrm{in}}-\sum \mathrm{d}m_{\mathrm{out}}\cdot h_{\mathrm{out}}+\mathrm{d}W \quad (71)$$

Using an instantaneous and stable process of the flow from the control volume, it can be set $h = h_{\mathrm{e}}$. Additionally, $h = c_{\mathrm{p}}T$, $\mathrm{d}Q = 0$, $\mathrm{d}W = -p\mathrm{d}v_{\mathrm{C}}$, and Equation (71) becomes:

$$\mathrm{d}(m\cdot u)=-pdv_C+c_p\sum T_{\mathrm{in}}\mathrm{d}(m_{in})-c_p\cdot T\sum \mathrm{d}(m_{\mathrm{out}}) \quad (72)$$

According to $\theta=\omega\cdot t$ (angular displacement), Equation (72) is now:

$$\frac{\mathrm{d}T}{\mathrm{d}\theta}=-\frac{(k-1)\,T}{v_C}\cdot\frac{v_C}{\mathrm{d}\theta}+\frac{k}{m}\cdot\left(k\cdot\frac{T_{in}}{T}-1\right)\cdot\frac{\mathrm{d}m_{\mathrm{in}}}{\mathrm{d}\theta}-\frac{(k-1)\,T}{m}\cdot\frac{\mathrm{d}m_{\mathrm{out}}}{\mathrm{d}\theta} \quad (73)$$

## 4.2 | Leakage equation

The radial leakage, through a clearance between the bottom (or the top) plate and the scrolls, and the flank leakage, through a clearance between the flanks of two scrolls, are the two machinery leakages.[17] The clearances are illustrated in Figure 21. According to the nozzle leakage model, the radial leakage can be expressed by Liansheng equation (1998):

$$\frac{\mathrm{d}m_{\mathrm{leak\_in\_axial}}}{\mathrm{d}\theta}=-\frac{\Phi_{\mathrm{axial}}\cdot\rho_{\mathrm{in}}(\theta)\cdot c_{\mathrm{axial}}\cdot L_{\mathrm{in\_radial}}(\theta)}{\omega}\times\sqrt{\frac{2k}{k-1}\cdot R\cdot T_{\mathrm{in}}(\theta)\cdot\left[1-\left(\frac{p_{\mathrm{in+1}}(\theta)}{p_{\mathrm{in}}(\theta)}\right)^{\frac{k-1}{k}}\right]}, \quad (74)$$

where $r$ is the inlet fluid density; $L$ is the length of leakage clearance; $\Phi$ is the flow coefficient; $c$ is the average leakage clearance and $\theta$ is the angular displacement. The flank leakage is given by.

$$\frac{\mathrm{d}m_{\mathrm{leak\_in\_radial}}}{\mathrm{d}\theta}=-\frac{\Phi_{\mathrm{radial}}\cdot\rho_{\mathrm{in}}(\theta)\cdot c_{\mathrm{radial}}\cdot h}{\omega}\times\sqrt{\frac{2k}{k-1}\cdot R\cdot T_{\mathrm{in}}(\theta)\cdot\left[1-\left(\frac{p_{\mathrm{in+1}}(\theta)}{p_{\mathrm{in}}(\theta)}\right)^{\frac{k-1}{k}}\right]}. \quad (75)$$

With $h$ = fluid enthalpy per unit mass, while the change of mass in the control volume can be calculated as follows:

$$\mathrm{d}m_{\mathrm{in}}=\mathrm{d}m_{\mathrm{leak\backslash\_in\backslash\_radial}}+\mathrm{d}m_{\mathrm{leak\backslash\_in\backslash\_axial}} \quad (76)$$

$$\mathrm{d}m_{\mathrm{out}}=\mathrm{d}m_{\mathrm{leak\backslash\_out\backslash\_radial}}+\mathrm{d}m_{\mathrm{leak\backslash\_out\backslash\_axial}} \quad (77)$$

All the working parameters of the expander can be found by solving Equations (74) and (75).

## 4.3 | Expansion ratio

With integer (n) expansions pockets, the expansion ratio is:

$$\beta^*=\left[\frac{(2n-1)}{\left(1+\frac{\theta_s}{\pi}\right)}\right]^k \quad (78)$$

Or:

$$\beta^*=\left[\frac{\left(2N-1-\frac{\theta^*}{\pi}\right)}{\left(1+\frac{\theta_s}{\pi}\right)}\right]^k \quad (79)$$

where $N = \mathrm{Int}(n) + 1$ and $\theta^* = 2p[1 - (n - \mathrm{Int}(n))]$.

## 4.4 | Delivery flow rate Q

The most diffused shape of the scrolls is an involute of a circle. Both spirals develop from the same circumference. The two circumferences are spaced by a constant gap. In Figure 26, φ represents the generic involute angle, which defines the coordinates of each inner and the outer profiles point (($x_{in}$, $y_{in}$) and ($x_{out}$, $y_{out}$), respectively), $\alpha_{in}$ and $\alpha_{out}$ are the starting position angles of the inner and the outer involutes, $r_b$ is the radius of the basic circumference, $r_c$ is the radius of the circular arc forming the inner portion of the scrolls and, finally, $\alpha_{in\_s}$ and $\alpha_{out\_s}$ are the initial angles of the inner and the outer spirals respectively. The equations, to calculate the volume of the chambers, are derived and fully described in Chen and Halm.[20,21] The suction volume, as a function of the shaft angle $\theta$, is expressed by:

$$V_s(\theta)=\frac{1}{2}\cdot h_s\cdot r_b\cdot r_0\cdot\left[2\varphi_e\theta-\theta^2-\theta\left(\alpha_i+\alpha_0+\pi\right)+2\cdot(1-\cos\theta)-2\cdot\left(\varphi_e-\pi\right)\operatorname{sen}\theta-\frac{\alpha_i+\alpha_0}{2}\cdot\operatorname{sen}(2\theta)\right] \quad (80)$$

where $h_s$ is the height of the chambers, $r_o$, is the radius of the orbiting circular path and $\varphi_e$ is the the ending angle of the involutes.

Compression chambers are built-in $C_{max}$ couples, where $C_{max}$ depends on the length of the wraps. The outer levels (until $C_{max}-1$) exist for the whole working cycle, the $C_{max\text{-}th}$ opens to the discharge region with a defined orbiting angle $\theta_d$. The volume of a $C^{th}$ level compression chamber is defined:

$$V_C(\theta)=\pi\cdot h_s\cdot r_b\cdot r_0\cdot\left\{2\varphi_e-2\theta-\left[\alpha_i+\alpha_0+(4C-1)\cdot\pi\right]\right\} \quad (81)$$

The discharge region is formed by three different chambers: the lateral ones $V_d$ and the inner zone $V_{dd}$, directly connected to the discharge hole. This volume reaches his minimum at $\theta_d$: that is the clearance volume $V_{cl}$. The discharge process begins at $\theta_d$, when the two $C_{max\text{-}th}$ level chambers open to the discharge region. The gap between scrolls is initially too small to achieve a pressure equalization, so the three chambers have to be treated separately. When the pressure equalization is reached, a unique discharge zone $V_d - V_{dd}$ must be considered. $V_{cl}$ is defined:

$$V_{cl}=h_s\cdot r_c^2\cdot\left[\pi-arc\operatorname{sen}\left(2\frac{r_b}{r_c}\right)-2\frac{r_b}{r_c}\right] \quad (82)$$

And the discharge volume is:

$$\left(V_d-V_{dd}\right)=h_s\cdot r_b\cdot r_0\cdot\left[\varphi_{C^2}\cdot-\left(\varphi_{os}+\pi\right)^2-\left(\pi+\alpha_i+\alpha_0\right)\cdot\left(\varphi_C-\varphi_{os}-\pi\right)\right]+V_{cl} \quad (83)$$

where $\varphi_{C^2}$ is the involute angle of the innermost contact point between scrolls, is defined:

$$\begin{cases}\varphi_{C^2}=\varphi_e-2\pi C_{max}-\theta\rightarrow\theta\le\theta_d\\ \varphi_{C^2}=\varphi_e-2\pi\left(C_{max}-1\right)-\theta\rightarrow\theta_d\le\theta\le2\pi.\end{cases} \quad (84)$$

The inner discharge volume is:

$$V_{dd}(\theta)=h_s\cdot r_c\cdot\left[r_c\cdot\beta-\left(r_c-\left(w_d-w_{dd}\right)\right)\operatorname{sen}\beta\right] \quad (85)$$

$\beta$ is a practical coefficient, introduced to simplify the calculation:

$$\beta(\theta)=\pi-arc\cos\left[\frac{r_c+r_0+r_0\cos\left(\theta-\theta_0\right)}{\left(r_c-\left(w_d-w_{dd}\right)\right)}\right]-arc\operatorname{sen}\left(2\frac{r_b}{r_c}\right). \quad (86)$$

The term ($w_d - w_{dd}$) represents the width of the opening between the discharge regions:

$$\left(w_d-w_{dd}\right)_{(\theta)}=r_c-\sqrt{r_0^2+\left(r_c-r_0\right)^2+2r_0\cdot\left(r_c-r_0\right)\cos\left(\theta-\theta_d\right)}. \quad (87)$$

The lateral discharge volume is:

$$V_d(\theta)=\frac{1}{2}\cdot\left[\left(V_d-V_{dd}\right)_{(\theta)}-V_{dd(\theta)}\right] \quad (88)$$

## 4.5 | Volumetric efficiency

This parameter is defined as the ratio of theoretical delivery to the practical delivery as follows: $\eta_v = V_{th}/V_s$.

$V_{th}$ is the volume of the control volume at the end of the charging phase and 0° rotation angle. The two primary factors affecting the volumetric efficiency are the leakage and the porting. The effect is a charging pressure decrease, lower than the nominal suction pressure. Consequently, a reduction of the inlet flow rate is checked. Finally, a flow chart of the design procedure (Figure 27a) and the different efficiency maps (Figure 27b) are presented.

# 5 | ROTARY VANE EXPANDER DESIGN PROCEDURE

The basic geometrical and kinematic characteristics are a function of the angular displacement of the expander's rotor. The parameters needed include:

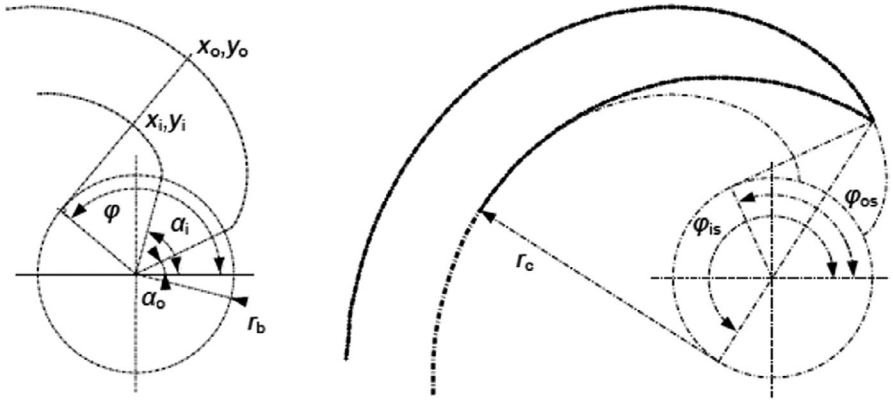


**FIGURE 26** Reference scheme for swept volume calculation

1. Variation of the cell volumes.
2. Volume expansion ratio, $r_v = V_2/V_1$ (Figure 28).
3. Variations of the protrusions of the vanes outside their rotors slots.
4. Vane sliding velocity.
5. Vane accelerations.

The first model's difference resides in the vane thickness calculations. In many other types of research, a vane thickness equal to zero has been assumed, for calculating the vane (cell) volume. According to recent work,[23] a circular stator cylinder has been considered, and a vane thickness is considered. Two arcs ($2\pi - \theta_{seal}$ and $\theta_{seal}$) can be checked. If the sealing arc is symmetric about the baseline ($\theta = 0$), it turns out that $\psi = 180°$ and RS($\theta$) = 180° (see Figure 22). Neglecting the thickness of the vanes and assuming in continuous contact between vanes and the stator cylinder, the ideal volume can be written as[22]:

$$V_{cy\_vanes}(\theta) = [A_{cy\_vanes}(\theta) - A_{cy\_vanes}(\theta, \delta)] \quad (89)$$

where $A_{cy\_vanes}(\theta)$ and $A_{cy\_vanes}(\theta - \delta)$ are the enclosed areas between the stator and rotor cylinders. The values of $A_{cy}$ are usually numerically solved.[22,24,25] The actual machine volume differs due to the presence of the extended portions of the leading and trailing vanes. The vanes are assumed to be rigid. $R(\theta)$ is defined as the radius of the stator cylinder to the center of the rotor as a function of angular displacement. For a circular stator cylinder this quantity is:

$$R(\theta) = e \cdot \cos(\psi - \theta) + \sqrt{r_R^2 + e^2 - 2 \cdot e \cdot r_R \cdot \cos\psi - e^2 \cdot \text{sen}^2 \cdot (\psi - \theta)} \quad (90)$$

where $\psi$ is defined as the angle between the arc and the rotor center. The vane protrusion can be calculated:

$$X(\theta) = R(\theta) - r_R \quad (91)$$

Vane velocity and acceleration can be computed, as follows:

$$v(\theta) = \dot{X}(\theta) \quad (92)$$

$$a(\theta) = \ddot{X}(\theta) \quad (93)$$

## 5.1 | Thermodynamic model

The thermodynamic model described in[26] is the foundation of the vane expander analysis. The model is based on the

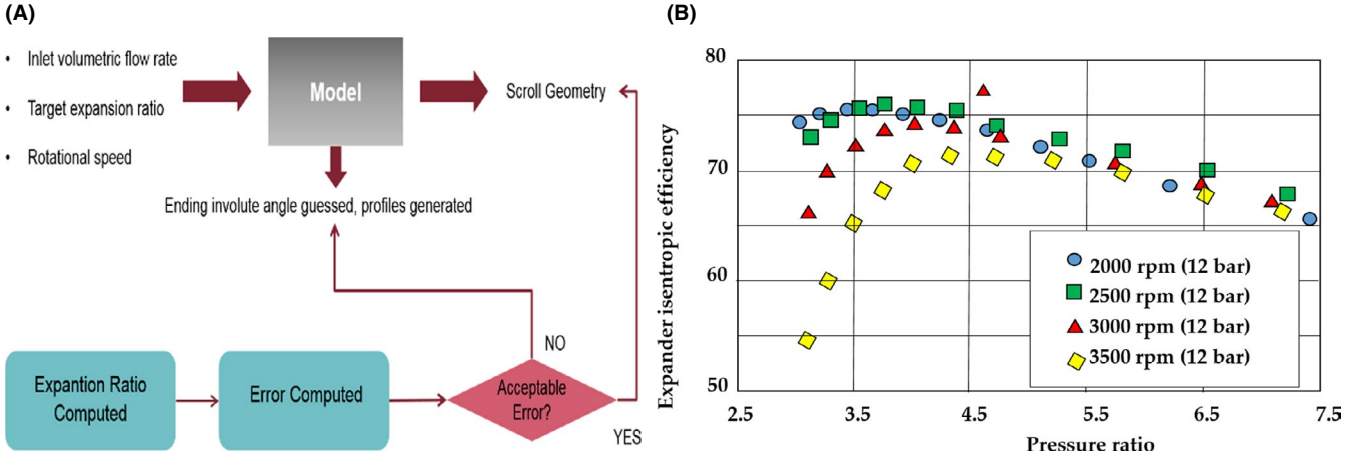


**FIGURE 27** A, Flow chart of design procedure. B, Reworked efficiency/pressure map[8]

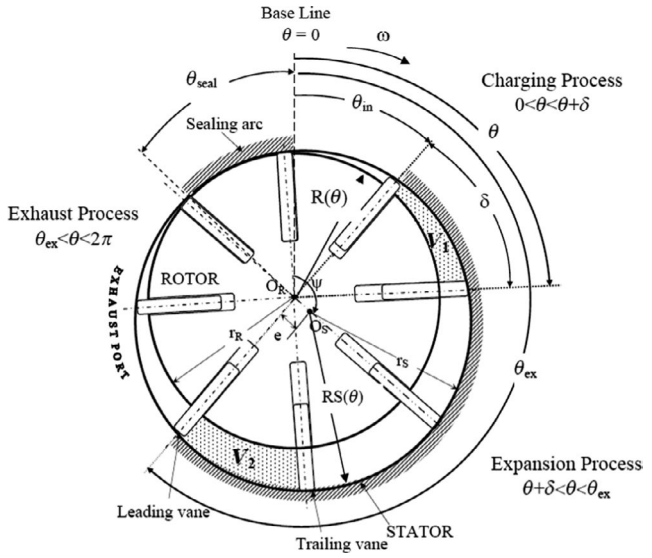


**FIGURE 28** Schematic of a rotary-vane [adapted from 24]

energy and mass conservation equation, applied to the control volume. Also, geometry machine design equations and the steam state equation are used. The system of differential equations is resolved numerically, providing the basic values of heat exchange.[27] Thus:

$$\dot{Q}-\dot{W}+(\dot{m}\cdot h)_{\text{in}}-(\dot{m}\cdot h)_{\text{out}}=\dot{U} \tag{94}$$

This model provides the ideal power value, where the mass transfer occurs through the inlet and discharge ports, and the control volume is adiabatic. The model also calculates the heat exchange. The losses can be evaluated with separate models. Once the losses percentages values are obtained, these values are inserted into the initial model and the calculation is carried out. Therefore, inlet and outlet flow rates include porting losses. Equation (92) calculates the indicated work or the work *pdv* made by the working fluid. Friction losses can be determined by a separate model. Once obtained, these values can be subtracted to the indicated work. To analytically determine the characteristics of the expander in the presence of leakage, friction, and heat transfer, separate models for these phenomena have been developed.

### 5.1.1 | Charging process

At angular displacements of $0 \le \theta < \theta + \delta$, the charging process occurs. The inlet fluid temperature can be determined from the degree of fluid superheated. The saturation pressure corresponding to the saturation temperature of the evaporator, the state of the fluid entering the expander can also be determined. The mass flow rate of the working fluid, assuming steady flow and neglecting changes in potential energy, can be written as:

$$\dot{m}_{\text{in}}(\theta)=\rho_{\text{ent}}\cdot C_{\text{d}}\cdot A_{\text{ent}}(\theta)\cdot V_{\text{ent}} \tag{95}$$

where the discharge coefficient "$C_{\text{d}}$" is assumed to be unity initially and will be determined by experimental data. The inlet throat area varies as a function of angular displacement and was found to obey the linear approximation.[26] The mass flow rate contained in the expander cell at any angular displacement is:

$$\dot{m}_{\text{cv}}(\theta)=\dot{m}_{\text{cv}}(\theta=0)+\int_0^{\theta}\frac{\dot{m}_{\text{cv}}(\theta)}{n}\cdot \text{d}\theta \tag{96}$$

Using Equation (94) it can be written:

$$\frac{\text{d}E_{\text{cv}}}{\text{d}t}=\dot{Q}-W+\dot{m}_{\text{ent}}h_{\text{ent}} \tag{97}$$

neglecting the changes in kinetic energy and potential energy, it is obtained $E_{\text{cv}} = \text{d}U_{\text{cv}}$. The pressure within the control volume is also assumed to be uniform. Multiplying by dt and neglecting friction, internal leakage losses and heat transfer, Equation (94) becomes:

$$\Delta U=-p_1\cdot\left(V_2-V_1\right)+\dot{m}_{\text{ext}}h_{\text{ext}} \tag{98}$$

The internal energy is:

$$u_2=\frac{m_1u_1-p_1\left(V_2-V_1\right)+m_{\text{ent}}h_{\text{ent}}}{m_2} \tag{99}$$

The fluid density is calculated as $r_2 = m_2/V_2$. The charging process is assumed to be a constant pressure process ($p_1 = p_2 = p_{\text{ent}}$). The mass, in the control volume, is unknown yet. In this case, the first law can be written as follows:

$$\Delta U=m_2u_2-m_1u_1=-p_1\cdot\left(V_2-V_1\right)+\left(m_2-m_1\right)h_{\text{ent}} \tag{100}$$

Substituting the density definition, previously described, into Equation (100) it is obtained:

$$\rho_2V_2u_2-m_1u_1=-p_1\cdot\left(V_2-V_1\right)+\left(\rho_2V_2-m_1\right)h_{\text{ent}} \tag{101}$$

where $\rho_2$ and $u_2$ are the unknowns. By neglecting temperature gradients within the control volume, these two unknowns may be determined by iterating on the temperature of the control volume that corresponds to the known pressure, $p_2$, and simultaneously satisfies the energy conservation Equation (101).

### 5.1.2 | Expansion process

During the expansion process, $\theta_{\text{in}} + \delta \le \theta < \theta_{\text{ex}}$, the mass in the control volume, $m_{\text{cv}}$, is constant after the "cut-off" angle

$\theta_{cut} = \theta_{in} + \delta$ where $\theta_{in}$ is the spread of the intake port and $\delta$ is the angle between successive vanes (eg $\delta = 45o$ for an eight-vane expander). By neglecting internal leakage losses, the mass in the control volume, $m_{cv}$, is assumed to be constant throughout the expansion process. If pressure gradients within the control volume, changes in kinetic and potential energy, friction and heat transfer are also neglected and the process may be considered isentropic, hence $s_2 = s_1$. The density is $r_2 = m_{cv}/V_2$. So the new thermodynamic properties, namely temperature, pressure, and quality, can be calculated from the isentropic process and density determination.

### 5.1.3 | Exhaust process

The exhaust process occurs at an exhaust angle $\theta_{ex} < \theta < \theta_{out} + \delta = \theta_{end}$, where $\theta_{out}$ is the exhaust port spread angle and $\delta$ is the angle between consecutive vanes. During the exhaust process, the working fluid mass flow rate discharged from the control volume as a function of angular displacement can be determined with the following equation:[26]

$$\dot{m}_{ex}(\theta) = \rho_{cv} \cdot C_{d,ex} \cdot A_{ex}(\theta) \cdot V_{ex} \tag{102}$$

where $\rho_{cv}$ is the density of the working fluid in the control volume at the current time step. The discharge coefficient, $C_{d,ex}$, is an empirically determined constant that takes into account exit port losses. Here, the discharge coefficient is assumed to be unity. The amount of mass contained in the control volume at any angular displacement can be calculated:

$$\dot{m}_{cv}(\theta) = \dot{m}_{cv}\left(\theta_{ex}\right) - \int_{\theta_{ex}}^{\theta} \frac{\dot{m}_{ex}(\theta)}{n} \cdot d\theta \tag{103}$$

where $\theta_{ex}$ is the angle at the end of the expansion process. As previously reported, the first law can be written as:

$$\frac{dE_{cv}}{dt} = \dot{Q} - W + \dot{m}_{ex} h_{ex} \tag{104}$$

By neglecting any kinetic and potential energy changes, it is obtained $E_{cv} = U_{cv}$. The exhaust process is at constant pressure ($p_{cv}(\theta_{ex}) = p_{ex}$) and in a quasi-equilibrium manner. Neglecting friction, internal leakage losses and heat transfer from the ambient, Equation (94) becomes:

$$\Delta U = -p_{ex} \cdot \left(V_2 - V_1\right) + m_{ex} h_{ex} \tag{105}$$

Applying the same solution methodology as in the charging process:

$$\rho_2 V_2 u_2 - m_1 u_1 = -p_{ex} \cdot \left(V_2 - V_1\right) + \left(\rho_2 V_2 - m_1\right) h_1 \tag{106}$$

where $\rho_2$ and $u_2$ are the unknowns. Neglecting temperature gradients within the control volume, these two unknowns may be determined by iterating on the temperature of the control volume that corresponds to the known pressure, $p_2$, and simultaneously satisfies the energy conservation equation.

### 5.1.4 | Ideal expander evaluation

For a given set of operating temperatures, the state of the fluid entering and leaving the expander may be determined. The process volume ratio is defined as:

$$r_{v,p} = v_{evap,in}/v_3 \tag{107}$$

where $v_3$ is the specific volume of the fluid at the condenser exit. The fluid may be a saturated or sub-cooled liquid at this state. This process volume ratio is expected to be smaller when the fluid leaving the condenser is sub-cooled. The built-in (or geometric) volume ratio of the expander can be defined as:

$$r_{v,b\_in} = \frac{v\left(\theta_{ex}\right)}{v\left(\theta_{in} + \delta\right)} \tag{108}$$

The built-in parameter and geometric volume ratios can be used interchangeably. If internal leakage losses are neglected, expander cell volumes ratio decreases, since the mass in the cell volume is constant. If the built-in volume ratio is lower, identical, or greater than the process volume ratio the blow-down, ideal expansion, and blow-back processes will occur, respectively. In the blow-back process situation, the higher downstream reservoir pressure generates a fluid flowing back into the expander, hindering the discharge process (Figure 23). A proper machinery design is mandatory for ensuring adequate operating conditions. To calculate the expander torque and power, the pressure forces acting on the vanes must be computed. If the pressure forces are applied at the vanes calculated protrusion midway point, the following expression for the torque, developed by one vane at any angular displacement, can be written

$$C(\theta) = X_v \cdot L \cdot \left[p_{cv}(\theta) - p_{cv}(\theta + \delta)\right] \cdot \left[r_R + \frac{X_v(\theta)}{2}\right] \tag{109}$$

If frictional losses are neglected, the average of the sum of the torque at any angular displacement multiplied by the

rotational speed is the generated expander power. The resultant power as a function of angular displacement is expressed as:

$$W(\theta)=\sum_{\theta=0}^{\theta=\theta+\delta}\frac{p_{in}\cdot\left(V_2-V_1\right)}{\Delta t}+\sum_{\theta=\theta+\delta}^{\theta=\theta_{ex}}\frac{m_{cv}\cdot\left(u_1-u_2\right)}{\Delta t}+\sum_{\theta=\theta_{ex}}^{\theta=2\pi}\frac{p_{ex}\cdot\left(V_2-V_1\right)}{\Delta t} \quad (110)$$

The appropriate selection of the expander geometry and rotational speed depends on the application. Usually, all preliminary operating parameters are tabulated.

## 5.2 | Friction model

The contact analysis between the several components of such machinery indicates that the friction losses are located in the following components:

a. Stator
b. Rotor
c. End plates

There is friction between the rotor and the endplates when rotor-end plate contact occurs. However, it was assumed that there was no rotor-end plate contact in the expander.

## 5.3 | Leakage model

Leakages can be taken into account by neglecting centrifugal effects and assuming the flow to be steady, laminar and incompressible. Often, the relative pressure drop is negligible since the leakage is often normal to the velocity in the regions where viscous dissipation occurs. The net pressure force on the side of the vane, $p_{vane}$, is:

$$p_{vane}=\left(p_{vane\_lag}-p_{vane\_lead}\right)\cdot A \quad (111)$$

where $p_{vane\_lag}$ and $p_{vane\_lead}$ are the pressures in the control volumes lagging and leading the vane and A is the exposed area of the vane. The pressures used are those predicted by the thermodynamic model in the presence of leakage but in the absence of friction. Due to the small vane-rotor clearance in a cold expander, it was assumed that $p_{vane}$ acts only on the vane in the space between the rotor and the stator and no other pressure forces act on the side of the vane. It was assumed that the pressure under the vane is the same in the leading control volume due to the pressure balancing ports.

The leakage flow paths that can be assumed for a single control volume, are shown in Figure 29. The leakage flow can be considered quasi-steady and laminar, due to the small

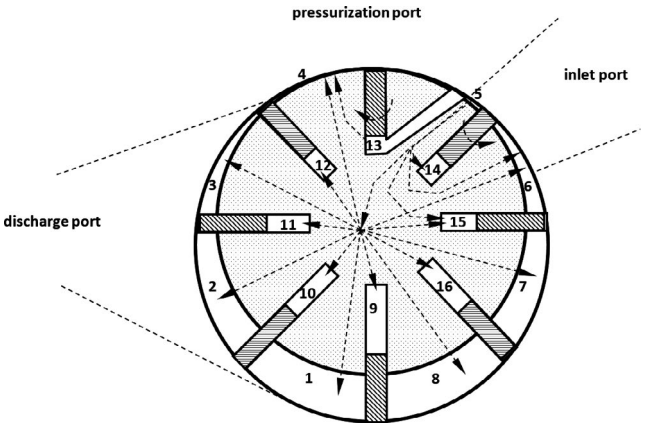


**FIGURE 29** Leakage paths for a considered Control Volume

clearances maintained in a vane expander. The first assumption is to study steam as an incompressible fluid. The relationship for parallel flow between flat plates was employed to obtain the following expression for the leakage flow along each path:

$$\dot{m}_{leakage}=\frac{\rho}{\mu}\cdot\frac{2\cdot\left(p_2-p_1\right)\cdot b^3\cdot w}{3\cdot\Delta x} \quad (112)$$

where $\Delta x$ is the lengths of the leakage paths, $w$ is the widths of the leakage paths, $b$ is the half clearance value between expander components, $\rho$ is the density and $\mu$ is the viscosity.

Then, $\Delta x$ is the straight line distance from the source to the sink along the leakage path. Equation (112) neglects relative motion between the moving and stationary parts. It can be applied to all the leakage paths. The pressures have been obtained as a function of the rotor position from the thermodynamic model.

## 5.4 | Heat transfer

### 5.4.1 | One-dimensional model

The heat transfer between the working fluid and the stator as well as between the working fluid and the endplates was performed to obtain an estimation of the effect of heat transfer on the expander performance. To evaluate the fluid motion, a flat plate model has been used. The standard relationships have been used to calculate the convective heat transfer coefficients. A typical electric analogy system calculation is adopted. In this case, the heat transfer rate is calculated as a function of several thermal resistances (component material, boundary layer, etc) and the temperature difference between the working fluid and the surrounding walls. The fluid operating temperatures are derived from the thermodynamic analysis. This simplified and preliminary heat exchange analysis does not permit an accurate determination of the temperature

profiles in the stator, rotor or endplate. A thermal expansion computational analysis is required. The assumption of this one-dimensional analysis supplies only approximate values. To improve the "confidence" on these results, more detailed and complicated models are necessary.

### 5.4.2 | Rotor—three-dimensional model

This approach is used to compute the heat conduction equation in the expander rotor. Considering a cylindrical coordinate system, it can write:

$$\frac{1}{\alpha}\cdot\frac{\partial T}{\partial t}=\frac{\partial^2 T}{\partial r^2}+\frac{1}{r}\cdot\frac{\partial T}{\partial r}+\frac{1}{r^2}\cdot\frac{\partial^2 T}{\partial \theta^2}+\frac{\partial^2 T}{\partial z^2} \tag{113}$$

Note that, in Equation (113), the heat transfer coefficient should be experimentally determined.

Since the flow pattern in the control volume is not known, it is difficult to determine the heat transfer coefficient between the steam and the rotor. Therefore, experimental tests can supply the measurement of the surface temperature, which can be considered a boundary condition on the rotor surface. Some researchers suggested assuming, for a given control volume, that the rotor surface temperature did not vary in the axial or tangential direction. This assumption does not consider the heat generated by friction between the vane and the rotor. To calculate the heat generated, a friction model is used. A fraction of the generated heat is transferred into the rotor and the remainder is moved to the vane. To have the exact amounts of heat, the temperature profiles in two semi-infinite solids in frictional contact must be computed. This temperatures relationship, at the surface of contact, is proposed[28]:

$$\dot{q}_1=\left[\frac{\ddot{q}_{\text{total}}}{1+\frac{k_1}{k_2}\cdot\sqrt{\frac{\alpha_2}{\alpha_1}}}\right]\cdot\frac{k_1}{k_2}\cdot\sqrt{\frac{\alpha_2}{\alpha_1}} \tag{114}$$

$$\dot{q}_2=\left[\frac{\ddot{q}_{\text{total}}}{1+\frac{k_1}{k_2}\cdot\sqrt{\frac{\alpha_2}{\alpha_1}}}\right] \tag{115}$$

For the vane portion not in contact with a vane, an adiabatic configuration is assumed. The rotor is axially symmetric. in the axial direction. Only rotor half axial length was used in the analysis. The rotor had an adiabatic condition at the plane of symmetry. Moreover, no friction is considered, thanks the rotor is not in contact with the endplate. The viscous energy dissipation between the oil and rotor only increased the temperature of the oil.

### 5.4.3 | Stator—three-dimensional model

The profiles and heat transfer rates, a three-dimensional analysis of the stator was required. The location of the inlet and exhaust ports at the axial center of the stator affect the calculations. The ports act as heat sources or sinks, causing temperature gradients between the ports and the stator. The three-dimensional steady-state heat conduction Equation (113) can be used again. At the inside surface, heat

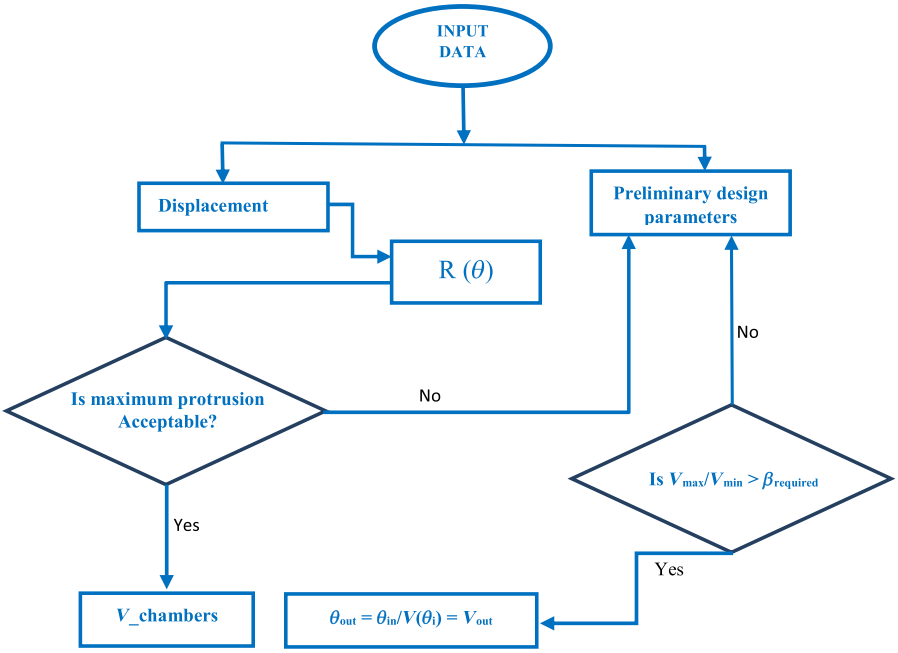


**FIGURE 30** Flow chart of Rotary Vane Expander design procedure

is transferred to the stator by convection. Additionally, the heat is generated at the inside surface due to friction between the vanes and the stator. To permit a steady-state analysis, the time-averaged wall temperature and heat generation rates are considered. The amount of frictional heat entering the stator and the vane was computed using Equation (115). An estimate of the convective heat transfer coefficient is obtained by modeling the flow over the stator as flow over a constant temperature semi-infinite flat plate. In this case, it is necessary to evaluate the coefficient "*h*." depending on the cases, for example, laminar or turbulent flow, with the usual formulae, previously discussed. Figure 30 shows the flow chart fo design procedure, while Figures 31 and 32 report the efficiency in function of the pressure ratio. This modified map has been used for the performance computation in the model.

## 6 | PISTONS EXPANDER DESIGN PROCEDURE

A piston expander is composed of a cylinder Z with an internal diameter *D* (bore), where a piston *S*, moved by a crank gear, completes its stroke (Figure 33). Generally, it is ordinary and balanced (not-balanced crank gears are not-frequent) composed by a connecting rod "b" and a crank "m." If the engine is multi-cylinder, the driving shaft can have more crankpins (crankshaft). The chamber volume is defined as the difference between the maximum volume (at the BDC) and the minimum one (at TDC). The piston displacement between the two dead centers is the stroke C. The compression and the expansion are due to these chamber volume variations, they require a short time to evolve and it is possible to consider these phases as adiabatic ones.

Considering the mechanism in the figure, the displacement variation can be so computed:

$$AA' = l\sin\varphi = R\sin\varphi \tag{116}$$

where

$$l = \mu R; \quad \beta = \frac{b}{l}; \quad \text{with} \quad \beta = 0 \div 1 \text{ and } \mu = 3 \div 4 \tag{117}$$

So:

$$\sin\varphi = \frac{\sin\theta}{\mu}; \cos\varphi = \sqrt{1 - \frac{\sin^2\theta}{\mu^2}} = \left(\mu - \frac{\sin^2\theta}{2\mu}\right) \tag{118}$$

The displacement is:

$$x = R\cos\theta + b\cos\varphi \tag{119}$$

$$y = (1-b)\sin\varphi \tag{120}$$

Substituting

$$x = R\left[\cos\theta + \beta\left(\mu - \frac{\sin^2\theta}{2\mu}\right)\right] \tag{121}$$

$$y = R(1-\beta)\sin\theta \tag{122}$$

Differentiating respect to the time, considering that $\omega = \mathrm{d}\theta/\mathrm{d}t$ the components of velocity and acceleration are:

$$\begin{aligned} u_x &= \mathrm{d}x/\mathrm{d}t = -R\left(\sin\theta + \frac{\beta}{2\mu}\sin 2\vartheta\right)\frac{\mathrm{d}\theta}{\mathrm{d}t} \\ &= \omega R\left(\sin\theta + \frac{\beta}{2\mu}\sin 2\vartheta\right), \end{aligned} \tag{123}$$

$$\begin{aligned} u_y &= \mathrm{d}y/\mathrm{d}t = -R(1-\beta)\cos\theta\frac{\mathrm{d}\theta}{\mathrm{d}t} \\ &= \omega R(1-\beta)\cos\theta, \end{aligned} \tag{124}$$

$$\begin{aligned} a_x &= \mathrm{d}^2x/\mathrm{d}t^2 = -R\left(\sin\theta + \frac{\beta}{2\mu}\sin 2\vartheta\right)\frac{\mathrm{d}^2\theta}{\mathrm{d}t^2} \\ &-R\left(\sin\theta + \frac{\beta}{2\mu}\sin 2\vartheta\right)\left(\frac{\mathrm{d}\theta}{\mathrm{d}t}\right)^2, \end{aligned} \tag{125}$$

$$\begin{aligned} a_y &= \mathrm{d}^2y/\mathrm{d}t^2 = -R(1-\beta)\cos\theta\frac{\mathrm{d}^2\theta}{\mathrm{d}t^2} \\ &-R(1-\beta)\cos\theta\left(\frac{\mathrm{d}\theta}{\mathrm{d}t}\right)^2. \end{aligned} \tag{126}$$

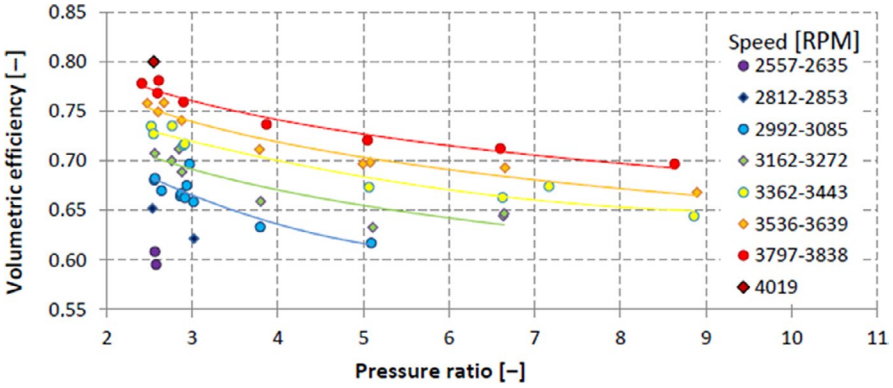


**FIGURE 31** Efficiency map in function of pressure ratio[17]

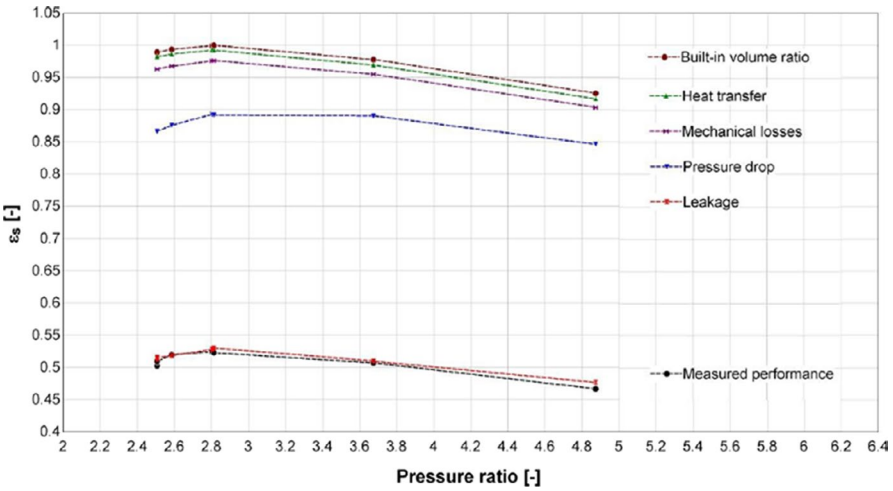


**FIGURE 32** Isentropic efficiency in function of pressure ratio

But $\omega = d\theta/dt = \text{constant}$ and $d^2\theta/dt^2 = 0$, so:

$$a_x = -\omega^2 R\left(\cos\theta + \frac{\beta}{\mu}\cos 2\vartheta\right) \tag{127}$$

$$a_y = -\omega^2 R(1-\beta)\sin\vartheta \tag{128}$$

Regarding the balancing of acting forces, Figure 34 shows the distribution. In stationary condition and neglecting the connecting rod mass, the force F can be split into two components:

$$F_b = F/\cos\varphi; N = \mathrm{F}\tan\varphi \tag{129}$$

The connecting rod is subjected to traction/compression stress $F_b$, while thrust $N$, perpendicular to the motion direction, does not add any other useful load. Such force by pushing the piston against the cylinder generates resistance by friction. The $N$ force and its corresponding $N_0$ (applied on the bench bearing) produce a variable intensity reaction torque, equal to the engine torque. On the frame also acts like an $F$ force perpendicular to $N_0$ and equal, in the module, to the force on the piston. In summary, the acting forces on the mechanism are:

1. Torque M;
2. Reaction torque N-$N_0$;
3. $F_0$ force on bearing;
4. Force F on the piston.

Neglecting the frictional losses and the inertial forces, it is possible to obtain the torque M:

$$M = F\cdot R\cdot\left(\sin\theta + \frac{R}{2L}\sin 2\theta\right) \tag{130}$$

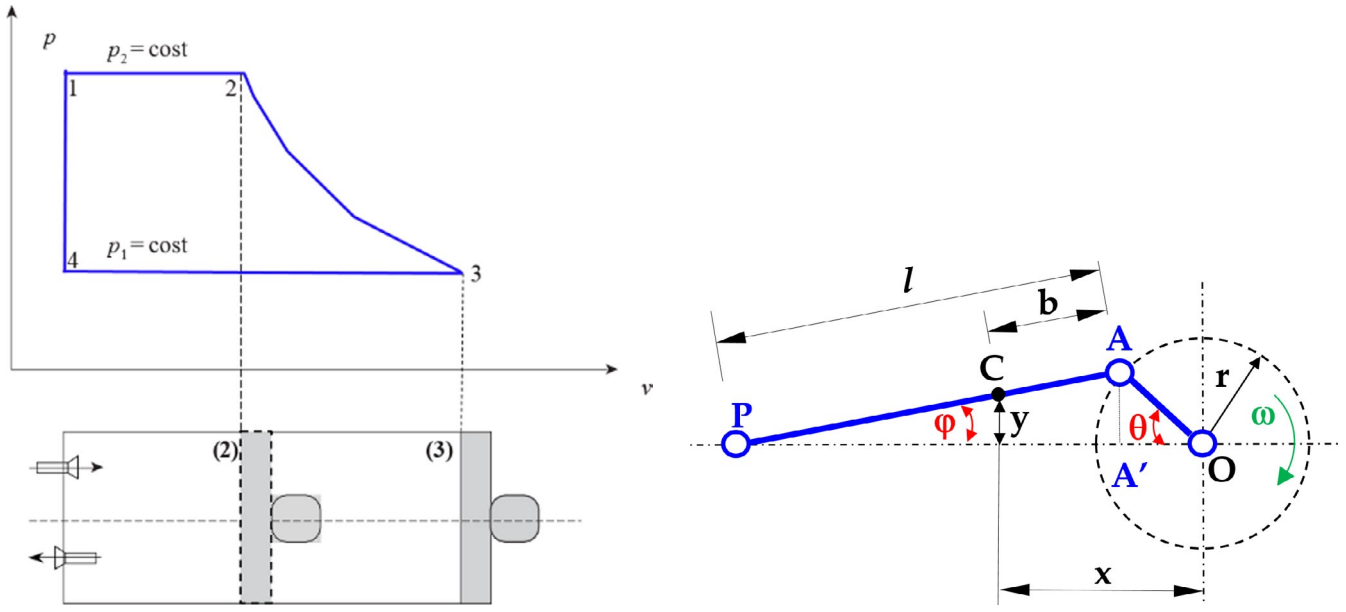


**FIGURE 33** The crank mechanism

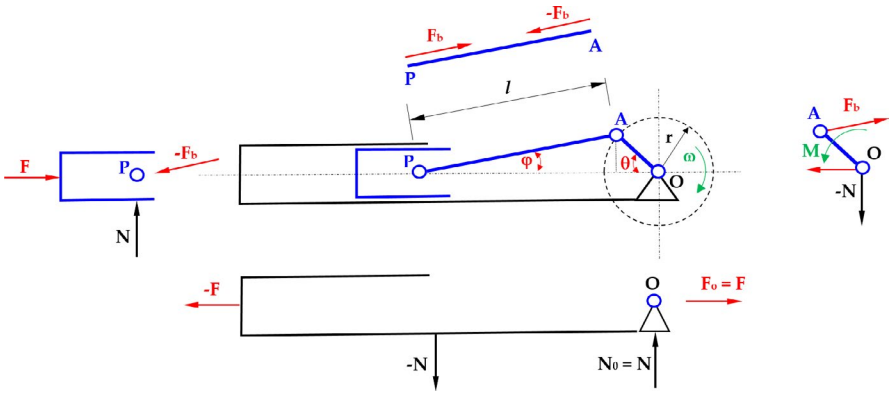


**FIGURE 34** Balancing forces for a crank mechanism

It is obvious that M is not constant, but it is null in the dead points. If *M* is too high, when the machine is stationary, it can prevent the starting of the operating machinery. In every point of the connecting rod, there is an acceleration due to the inertial force that stresses the mechanism. The transverse accelerations $a_y$ bend the connecting rod. They impair the tight joints and introduce many mechanical losses due to the sliding seating is not much lubricated and is very noisy. For these reasons, in huge machinery, the connecting rod is positioned slightly out of the cylinder to improve the kinematical connection and to decrease the frictions and so the crosshead is used but it increases the overall height of the machine.

For these reasons, the reciprocating machinery has two disadvantages: the *torque* and the *moment of resistance* are variable and a flywheel is often used to compensate for this variation; the *alternative forces* on bearings create stress and structure vibrations. The inertial forces of the piston and the connecting rod masses are characterized by an accelerating motion and they create other alternate forces balanced by some counterweights. These problems reduce the angular velocity of the machine. The flow rate of reciprocating machinery is:

$$Q = \eta_v \frac{1}{4}\pi D^2 C n \tag{131}$$

$\eta_v$ is the volumetric efficiency; for liquids $\eta_v \approx 1$, for gas $\eta_v = 0.65 \div 0.85$. For incompressible fluids $\eta_v < 1$ due to the hydraulic resistance in the suction piping (the pressure and the fluid density reservoir) and some fluid leaks through the seals. Besides, the effect of the noxious volume that reduces the available volume. The noxious volume cannot be null because it is necessary to avoid the piston impact on the cylinder head and allow the opening of the inlet and outlet valves.

Considering Figure 34, net power and work can be so computed.

The work along 1-2 transformation (vapor admission) is:

$$W_{1-2} = p_2 V_\varepsilon \tag{132}$$

where $V_\varepsilon$ is the admission volume ratio ($V_2$-$V_1$). The expansion work (2-3 process) is:

$$W_{2-3} = \frac{1}{k-1}\cdot p_2 \cdot V \cdot \left(\frac{1+\mu}{\varepsilon_{\exp}}\right)\cdot \varepsilon_{\exp}^{1-k} \tag{133}$$

where k = 1.13 for saturated vapor and 1.31 for reheated vapor. $\varepsilon_{exp}$ is the expansion ratio (depending on such a type of expansion is achieved, cfr par. 2.3) and μ is the noxious volume degree. If $C_C$ is the compression ratio, the volume of steam discharged in the forced discharge phase is $(1 - C_c)\cdot V$. Therefore, the extraction work will be:

$$|W_{3-4}| = p_1 \cdot (1 - C_C)\cdot V \tag{134}$$

The adiabatic compression work is:

$$|W_{4-1}| = \frac{1}{k-1}\cdot p_1 \cdot V \cdot (C_C + \mu)\cdot \left[\left(1+\frac{C_C}{\mu}\right)^{k-1} - 1\right] \tag{135}$$

The network is:

$$W = W_{1-2} + W_{2-3} + |W_{3-4}| + |W_{4-1}| \tag{136}$$

Diving (a) by the displacement, it is possible to calculate the limit mean pressure:

$$p_{lm} = p_2\alpha_{adm} - p_1(1 - C_C) + \frac{1}{k-1}\left\{p_2\frac{1+k}{\varepsilon_{esp}}\left(1-\varepsilon_{esp}^{1-k}\right) - p_1(C_C+\mu)\left[\left(1+\frac{C_C}{\mu}\right)^{k-1} - 1\right]\right\} \tag{137}$$

The power for a double-acting single cylinder is

$$P_{lim} = \frac{p_{ml}L_{lim}}{V} = p_{lm}Vn = \frac{1}{4}\pi D^2 C n \tag{138}$$

Introducing the loss coefficient "ζ" due to the presence of the plunger rod:

$$P_{lim} = p_{\mathrm{lm}} V (1-\zeta)\, n \tag{139}$$

From the Equation (136), it is clear that work value depends, in addition to the inlet and outlet pressures, on the admission and expansion degrees and $C_C$ parameter.[29,30,31,32] Note that, if the $\varepsilon_{\mathrm{adm}}$ increases (with the consequent reduction of $\varepsilon_{\mathrm{esp}}$) and $C_C$ decrease, the limit work increases. Nevertheless, it is equally clear that, at the same time, the internal performance of the expander is being reduced due to the loss of a larger part of the steam expansion work and for other losses. However, it is not uncommon for small mechanical drive machines, for which the power density than the performance is required, are built with a full admission ($\varepsilon_{\mathrm{adm}} = 1$) and without compression ($C_C = 0$). The steam consumption is calculated as follows. During each admission phase (constant pressure $p_2$) a quantity of steam equal to:

$$\dot{m}_{\mathrm{vap}} = \rho_{\mathrm{vap}} V b \tag{140}$$

where $\rho_{\mathrm{vap}}$ is the density of inlet vapor. The vapor is introduced for each chamber is:

$$\dot{m}_{\mathrm{vap}} = \rho_{\mathrm{vap}} V \varepsilon_{\mathrm{adm}} n \tag{141}$$

If the double-acting machine is considered:

$$\dot{m}_{\mathrm{tot}} = (2-\zeta)\, \rho_{\mathrm{vap}} V \varepsilon_{\mathrm{adm}} n \tag{142}$$

The specific consumption is derived as:

$$c_s = \frac{\rho_{\mathrm{vap}} \cdot \varepsilon_{\mathrm{adm}}}{p_{\mathrm{ml}}} \tag{143}$$

The plunger makes available an actual work and power, lower than the previous ones.

So, the actual expander efficiency is calculated, multiplying it by the mechanical efficiency that takes into account the overall losses:

$$\eta = \eta_{\mathrm{exp}} \eta_{\mathrm{mech}} \tag{144}$$

The $\eta_{\mathrm{mech}}$ is not very high (maximum load is between 0.6 and 0.9, from small to large sizes), mainly due to losses in the distribution devices. There is an empirical formula, from Krabak, valid for power between 35 and 220 kW, which defines mechanical performance as:

$$\eta = A + B \sqrt[2]{\frac{P_{\mathrm{ind}}}{p_{\mathrm{lm}}}} \tag{145}$$

where $A$ is about 0.85 ÷ 0.88 and $B$ is within 0.0040 ÷ 0.0036 (for condensation and free discharge machines). The expression of the actual power is calculable, for single-chamber double-acting machines multiplying the (140) and (141) for $\eta_{\mathrm{mec}}$. So the effective mean pressure is:

$$p_{\mathrm{me}} = p_{\mathrm{lm}} \eta_{\mathrm{mech}} \tag{146}$$

So that

$$P_{\mathrm{eff}} = \frac{1}{4} p_{\mathrm{me}} \pi D^2 C n = \frac{1}{4} p_{\mathrm{mi}} \pi D^2 C (1-\zeta)\, n \tag{147}$$

## 6.1 | Machinery losses

These losses can be divided into:

- Leakage losses;
- Dead volume vosses;
- EndWall losses;
- Incomplete expansion losses.

### 6.1.1 | LEAKAGE LOSSES

The steam pressure, acting on the plunger surface during the admission phase, is lower, due to the load losses in the internal piping. The difference is accentuated during the plunger's motion, which starts from its TDC accelerates towards the center of the cylinder; The actual 1-2 steam admission line, in the plane ($p$, $v$), has the trend different from that marked in Figure 33, resulting in a performance decrease. The leakage losses change the quality of the steam, as the frictional energy could increase its title and sometimes causing a slight overheating. When discharged, fluid pressure is maintained higher than that limit (Blow-Down) and the power and efficiency losses are not recoverable.[31,32] Finally, it is noted that the losses considered depending on the cubic power of the speed, so it is suggested not to use too fast expanders.

### 6.1.2 | DEAD VOLUME LOSSES

The dead volume cannot be eliminated, from a constructive point of view. It allows the opening and closing of the admission and exhaust port and the recovery of the clearances between the various moving parts. In steam machines, "water shots" due to condenses are dangerous. The working fluid becomes incompressible by generating unwanted dynamic actions on the various parts. In the case of incomplete expansion, at the beginning of each process, in the machine dead volume, the steam coming from the boiler would find the exhaust pressure $p_1$ and it would be

necessary to use a certain mass "m" of the vapor to reach the pressure $p_2$ before starting the introduction phase. This "m" amount of steam must compress the operating fluid up to the $p_1$ pressure, which exists in dead space. In this way, the fluid is introduced, in an adiabatic way, in an equal volume of:

$$V^* = V_d \left(\frac{p_2}{p_1}\right)^{-\frac{1}{k}} \tag{148}$$

In this way, the volume filled in $V_d$ is:

$$V_d - V^* = V_d \left(\frac{p_2 - p_1}{p_2}\right)^{1/k} \tag{149}$$

So, of the two quantities:

$$\frac{\left(\frac{\Delta p}{p_2}\right)^{1/k}}{\left(\frac{\Delta p}{p_2}\right)^{1/k} + \frac{V}{V_m}\varepsilon}; \frac{\frac{V}{V_m}\varepsilon}{\left(\frac{\Delta p}{p_2}\right)^{1/k} + \frac{V}{V_m}\varepsilon} \tag{150}$$

The first one loses its introduction work entirely, while the second uses its work. Losses increase proportionally $\mu$. To limit this leakage, the residual steam is compressed. Machines with a very high compression rating have been studied, thus characterized by high internal performance. Nevertheless, the rated power, compared to the displacement, is not satisfactory even for their single-acting operation.

### 6.1.3 | WALL LOSSES

During the admission phase, the working fluid, encountering the cold walls, can partially condense and deposit dew on the walls, that absorb heat and warm up. In the expansion phase, the pressure decrease vaporizes the deposited fluid and the state transition takes place at the expense of the previously absorbed heat. As the plunger moves, new areas of cold metal are discovered, producing additional condensations. At the same time, other condensations occur within the expanding fluid. The cylinder walls behave like thermal accumulators. Experimental measures have verified that evaporation generally prevails, but at the end of the expansion the vapor quality is always, quite low and liquid is still deposited on the walls. This loss, usually referred to as *loss by initial condensation*, consists of the fact that the vapor supplies to the walls heat at high temperature and then adsorbs it, totally or in smaller or even greater quantities, at a lower temperature, and in unavailable conditions. After the expansion, a sudden pressure decrease is produced in the cylinder and the liquid left on the walls evaporates promptly, subtracting heat from the walls themselves. On the other hand, the walls that "hold" it during the first expansion section and then delivered it, without any useful effect, receive some of the fluid thermal amount introduced into the cylinder. In some cases, this loss exceeds 40% of the available energy. The measures used to limit the thermal action of the walls are as follows:

1. Using overheated fluid (at least at 150-200°C, depends on the fluid) in admission, especially to reduce the effect of initial condensation thanks to the low thermal exchange coefficient in comparison to the very high condensing saturated fluid.
2. Increase the rotational speed of the machine, to reduce the time of thermal exchange.
3. Apply the so-called "Watt Jackets" to the walls. These jackets are crossed by working fluid and keep the wall temperature at a value higher than the admitting fluid one, limiting or drastically reducing the initial condensation.
4. Practice multiple expansion, reducing the fluid thermal excursion in each cylinder.
5. Consider extending the compression phase to increase the average temperature of the walls and the residual fluid.

### 6.1.4 | INCOMPLETE EXPANSION LOSSES

Pistons expanders cannot have a very prolonged steam expansion for obvious dimensional reasons, due to the high fluid specific volumes at low pressures. Therefore, the expansion is usually stopped before reaching the exhaust pressure in the cylinder. If the expansion were to be further extended, much of the obtained work would be spent on mechanical losses in cylinder-piston coupling. Interrupting the expansion results in the work loss: this loss depends on the $\varepsilon_{adm}$ parameter. This loss, called triangular loss, can be easily calculated[31,32,33] if the expansion extension is considered isothermal. Usually, assessing the overpressure of eight times of exhaust pressure, the loss is about 60 to 100 kPa. A flow chart of the design procedure is shown in Figure 35.

## 7 | A PROPOSAL FOR EXPANDER SELECTION CRITERION

To perform the final choice of the optimal expander, a good balance between several factors has to be found. For this reason, it was decided to use the code for filling out a table, with all the relevant issues to be addressed, and assign them a value from 1 (*less desirable*) to 3 (*more desirable*) for each Expander. The considered parameters for the choice are the following:

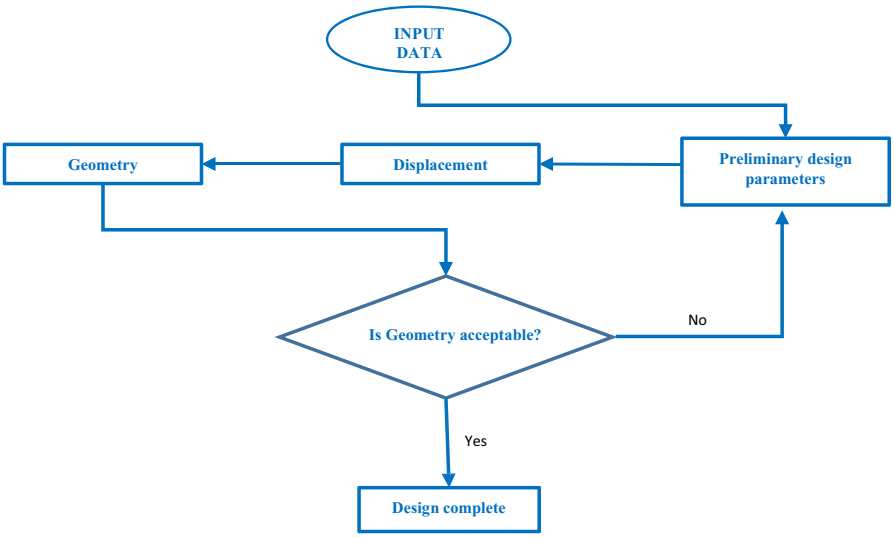


**FIGURE 35** Flow chart of Pistons Expander design procedure

*Efficiency*: Overall isentropic efficiency as described in each dedicated paragraph. Even if, as previously mentioned, no volumetric expander could challenge an IFR in terms of efficiency. Besides, both scroll and screw expanders have shown interesting efficiencies.

*Machinery volume*: Represents machine overall encumbrance. From this point of view, the turbine shows the optimal characteristics again. The screw expander has the greatest volume, while the scroll machine offers a good compromise between volume and efficiency.

*MTBF* (Mean Time Between Failure): this aspect considering all the moving parts. The scroll and the screw expander present just a few moving parts, which can either be in contact (if good lubrication is expected) or built with a clearance that does not decrease the machine efficiency and guarantees the absence of contact, thus reducing the wear damage. Moreover, the low rotational speed of the volumetric machines implies less stress on the bearings, with longer maintenance intervals and increasing their reliability.

*Lubrication*: While the turbine does not present any issues related to lubrication, the issues related to the screw motor can be relatively easily dealt with by choosing an unsynchronized configuration working with a good lubrication fluid. Both scroll and rotary vane expanders, to guarantee good reliability and longer life, should not be oil-free, thus an oil circuit has to be expected.

*EM coupling:* The simplicity of connection to an electric generator mostly depends on the rotational speed. In this case, the turbine is the least favorable.

*PLE* (Partial Load Efficiency): IFR turbines low flexibility makes their use undesirable in partial load applications. On the contrary, volumetric expanders show great flexibility and can operate smoothly under unsteady conditions. This is one of the main reasons that make those machines appealing to bottoming ORC waste heat recovery processes. The screw motor, in particular, has shown in literature an excellent behavior under unsteady conditions.

## 7.1 | Case study

The target cycle is an ORC plant, operates as a bottoming cycle of a common Diesel 8000cc engine for bus applications.[34] The steady-state condition of the exhausted gasses, after the supercharger turbine, are reported in Table 1.

The organic fluid R245fa was chosen because it is the most used organic fluids thanks to its reliability and its favorable performance in heat recovery systems. In fact, within a homologous series of chemical species, as chain length and molecular weight increase, the molar heat capacity and entropy increase. More specifically, with comparable latent heats, as the slope of the entropy lines decreases, the cycle efficiency will increase. Given the proportionality between the natural logarithmic of pressure and the inverse of temperature, the slope of the entropy line will be approximately the change in enthalpy with a change in temperature (for small changes in temperature), that is, the heat capacity. Even though R11, R123, and R245fa are not in the same homologous series, the longer molecular chain length of R245fa means that the vibrational component of heat capacity will increase as well the entropy due to the increased degree of freedom. These characteristics make R245fa one of the most appealing fluids for ORC applications. Regardless of the fluid choice, since R245fa is an HFC with a GWP greater than

**TABLE 1** ICE data

| $\dot{m}_{exhausted}$ (Kg/s) | $T_{exhausted}$ (K) | $p_{exhausted}$ (bar) |
|---|---|---|
| 0.8 | 800 | ≈1 |

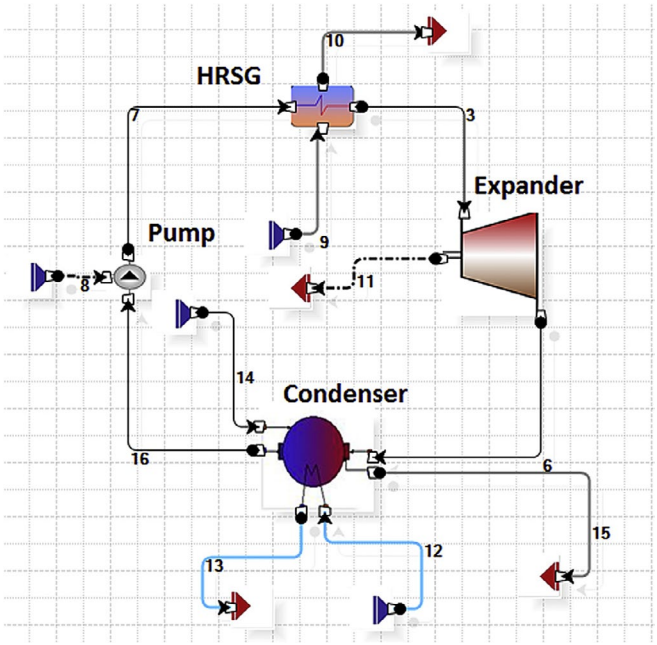


**FIGURE 36** Plant layout on Camel simulation code and definition of pitch point

1000 and important fluid banning are expected in the next years. The steady-state simulations of the plant have been performed using the CAMEL-Pro process simulator to analyze the system performance (Figure 36) and to choose the evolving mass flow rate concerning a reasonable cooling mass flow rate into the condenser. The CAMEL –Pro (Calculation by Modular Elements) software has been developed at the Department of Mechanical and Aerospace Engineering of the University of Rome "la Sapienza." It is written in C++, is based on an object-oriented approach and is equipped with a friendly user interface where the system is represented as a network of components connected by energy or flow streams,each component is characterized by a set of the equation, which describes the thermodynamic evolution imposed on the streams. The complete solution is available after having assigned the right boundary conditions.

Given the ICE working conditions, after having chosen a pitch point temperature $\Delta T_{pp} = 20°C$, the maximum working fluid mass flow rate has been evaluated as:

$$\dot{m}_{\mathrm{R245fa,\ max}} = \frac{\dot{m}_{\mathrm{exhausted}} cp' \left(T_4 - T_M - \Delta T_{pp}\right)}{h_0 - h_M} \cong 1.5\ \mathrm{Kg/s}.$$

To choose a correct value, as previously mentioned, a good balance between a high mass flow rate of the working fluid, which affects directly the power output, and a reasonable mass flow rate of the cooling water in the condenser has to be computed. The condenser is the bulkiest component, but in any case, it does not compromise the feasibility of an on-board system. The working fluid is first compressed to a maximum pressure of 1 MPa, then it is heated, evaporated and superheated up to 413 K in the HRSG (heat recovery steam generator) to be expanded down to 185 KPa and then re-condensed at 293 K. Pressure

**TABLE 2** Operating plant specifications

| Parameter | Quantity | Parameter | Quantity |
|---|---|---|---|
| $\dot{m}_{\mathrm{exhausted}}$ | 0.8 Kg/s | $T_{R245fa}$ at expander outlet | 368 K |
| $T_{\mathrm{exhausted}}$ at HRSG inlet | 800 K | $p_{R245fa}$ at expander outlet | 180 kPa |
| $T_{\mathrm{exhausted}}$ at HRSG outlet | 620.5 K | $T_{R245fa}$ at condenser outlet | 290 K |
| $p_{exhausted}$ at HRSG inlet | 101.3 kPa | $p_{R245fa}$ at condenser outlet | 177 kPa |
| $p_{exhausted}$ at HRSG outlet | 99.3 kPa | $\dot{m}_{\mathrm{water}}$ | 2.1 kg/s |
| $\dot{m}_{R245fa}$ | 0.5 kg/s | $T_{water}$ at condenser inlet | 293 K |
| $T_{R245fa}$ at HRSG inlet | 294 K | $p_{water}$ at condenser inlet | 101.3 kPa |
| $T_{R245fa}$ at HRSG outlet | 413 K | $T_{water}$ at condenser outlet | 308 K |
| $p_{R245fa}$ at HRSG inlet | 1000 kPa | $p_{water}$ at condenser outlet | 100 kPa |
| $p_{R245fa}$ at HRSG outlet | 980 kPa | $P_{net}$ | 18 kW |

**TABLE 3** Simulations results

| Machinery | Main specifications (all measures are in centimeters) | | | | | | | $\omega$ | $\eta$ |
|---|---|---|---|---|---|---|---|---|---|
| IFR | $D_1 = 7.7$ | $b_1 = 0.22$ | $D_{2,mid} = 3.8$ | $\beta_2 = 27°$ | $b_2 = 1.35$ | $D_{2,sh} = 5.12$ | $D_{2,hub} = 2.4$ | 4896 | 0.8 |
| Screw | $D = 18.4$ | $d = 11.41$ | $s = 11$ | | | | | 314 | 0.68 |
| Vaned (RVE) | Vanes = 8 | $r_R = 10$ | $e = 3$ | $h = 26$ | | | | 419 | 0.48 |
| Scroll | $r_D = 5.4$ | $D_{max} = 18$ | | $h = 10.2$ | $A_{in} = 22.3$[a] | $A_{out} = 121$ | | 314 | 0.7 |
| PE | $D = 13$ | $C = 15.6$ | | | | | | 314 | 0.78 |

[a]In $cm^2$

and temperature parameters are chosen in line with common ORC cycle parameters for the considered fluid in such of applications and to achieve a good compromise between a high enthalpic drop in the expander (maintaining the fluid far from the critical point) and an acceptable condensing temperature. The final expected working conditions are the ones illustrated in Table 2.

Once decided on the choosing parameters, several simulations have been conducted on a case study. These data are used to run the program. The simulation results of design procedures are briefly summarized in Table 3. All geometrical characteristics are referred to as the previous description in the text, as well as, the design procedure. For the assigned power value the code provided the characteristic dimensions of the machines. Once the various geometric parameters have been obtained, the primary code transfers the values to the second part of the program. This second part has a continuous updating library with all efficiency available map (commercial and tested[35,36,37,38,39] for all machinery, as well as, the various map of volumetric or mechanical efficiency versus rotational speed, the mass flow rate in function of working pressure, etc Thus, Table 4 can be compiled and the results are reported in Table 3. The value of MTBF is a code string compiled and assigned by the user, based on the experience and available reports.

According to this procedure, the screw machine turns out to be the optimal compromise for this purpose (small rated power plant). However, depending on the application, the relative weight of each device should be taken into account, thus making a general procedure of choice extremely challenging. Moreover, since ORC bottoming cycles for waste heat applications are in general not commercial, each component should be designed and manufactured ad hoc, making the investment highly demanding, and cost analysis should be carried on along with the design of each component.

**TABLE 4** Selection table for ORC expanders

| | IFR | Screw | Rotary Vane | Scroll | PE |
|---|---|---|---|---|---|
| Efficiency | 3 | 2 | 1 | 2 | 3 |
| Machine volume | 3 | 1 | 1 | 2 | 1 |
| MTBF | 2 | 3 | 2 | 3 | 3 |
| Lubrication | 3 | 3 | 2 | 1 | 1 |
| EM Coupling | 1 | 3 | 3 | 3 | 3 |
| PLE | 1 | 3 | 2 | 2 | 2 |
| TOTAL | **13** | **15** | **11** | **13** | **13** |

## 8 | CONCLUSIONS

This paper has analyzed in detail different expander configurations, namely a radial turbine, a scroll-type expander, a screw-type expander, a rotary vane expander, and a reciprocating expander, highlighting each different feature. For each component, the theory on which the choice is based has been described and its design has been presented.

The particular aspect of this work is the new approach to expander design procedure for small rated ORC. Once all the calculation procedures have been defined, they have been implemented in Matlab code. This code, once the design process is complete, indicates the optimal expander configuration to adopting to those specific systems. The expander choice is to be made accordingly to the ORC plant features like layout, size, power, expected operating time, and so on.

The implementation of this tool is not only useful at the level of a preliminary study of the ORC system and its components but can also provide useful guidance on the expander model to be used and the various possible competitors. Remember that the choice, sometimes, is dictated by design philosophies or external constraints, but in any case, this tool allows us to indicate the optimal machinery configuration, first of all, and then on the total size, weight, and efficiency.

In the presented case study, the tool indicates that the screw expander is the optimal choice. This indication is also supported by the various existing similar systems and by the numerous operating plants, which use such machinery. Finally, it is therefore believed that this tool is valid and can be further developed by inserting a large database. Future development could be to implement an expert system that guides, gradually, the designer.

## NOMENCLATURE

| | |
|---|---|
| *A* | Area (m2) |
| a | Acceleration (m/s2) |
| b | Blade height (§1), Half clearance value between expander components (§4) |
| BDC | Bottom Dead Center (§5) |
| C | Stroke [m] (§2), couples of spirals (§3), torque (§4) |
| c | Average leakage clearance [m] (§3) |
| Cd | Discharge coefficient (§4) |
| cp | Specific heat [J/kg K] (§3) |
| Csp | Spouting velocity [m/s] (§1) |
| D,d | Diameter [m] |
| E | Kinetic energy [J] (§4) |
| e | Eccentricity [m] (§4) |
| h | Enthalpy [J/kg K], chamber height [m] (§3) |
| IFR | Inward-Flow Radial |
| K | Corrective factor |
| k | Gas constant (§2), Heat transfer constant (§4) |
| L | Length [m] (§1), Length of leakage clearance [m] (§3), Vane length [m] (§4) |
| m | Mass flow rate (kg/s) |
| n | Rotational speed [rpm] (§2,4) Expansions pocket, chamber (§3) |
| p | Pressure (Pa) |
| Q | Heat (J), delivery flow rate [m3/s] (§3) |
| R,r | Radius [m], Radius of the stator cylinder to center of the rotor (§4) |
| r | volume expansion ratio (§4) |
| s | pitch [m] (§2) |
| T | Temperature [K] or [°C] |
| TDC | Top Dead Center (§5) |
| U | Blade Speed [m/s] (§1), Potential energy [J] |
| V | Real Flow Speed [m/s] (§1), Displacement [m3] (§2,3,4) |
| v | Velocity [m/s] (§1,2,4), Specific volume [$m^3$/kg] (§3) |
| W | Work [J], Relative Flow Speed [m/s] (§1), width [m] (§3), Widths of the leakage paths (§4) |
| X | Vane protrusion displacement (§4) |
| Z | Number of Blades (§1) |
| z | Number of wheels (§2), Axis coordinates (§4) |

### Greek symbol

| | |
|---|---|
| α | Real Velocity Angle [rad] or [°] (§1), Angle [°] (§2), Volutes angles [°] (§3), Conductibility [W/m] (§4) |
| α(T) | Temperature-Dependent Parameters |
| *β* | Pressure ratio (§2), Expansion ratio (§3), relative velocity angle [°] (§1) |
| *δ* | Blade blockage factor (§1), Procession angle [°] (§4) |
| *Φ* | Flow coefficient (§3) |
| *η* | Efficiency |
| φ | Flow Coefficient (§1), The ending angle of the involutes (§3) |
| κ | Gas constant (§3) |
| μ | Viscosity [P] (§4) |
| υ | Specific volume [m3/kg] (§4) |
| θ | Angular displacement (§ 3,4) |
| ρ | Density [kg/m3] |
| ω | Angular speed [rad/s] |
| ψ | Stage Loading (§1) |
| Ψ | Working angle [°] (§3) |
| Ωs | Specific Velocity(§1) |

### Subscripts

| | |
|---|---|
| 0 | Orbiting circular path(§3) |
| 1 | Inlet |
| 2 | Outlet |
| c | Inner spiral radius (§3) |
| cv | Control volume (§4) |
| cy | Cylinder (§4) |
| d | Defined orbiting angle (§3) |
| ent | Entering (§4) |
| evap | Evaporating (§4) |
| ex | Expansion process ending (§2), External (§4) |
| exp | Expansion (§1) |
| in | Inlet |
| leak | leakages (§3) |
| max | Maximum |
| mech | Mechanical (§2) |
| mid | Mid-span (§1) |
| out | Outlet |
| R | Rotors (§4) |
| s | Isoentropic (§2), General chambers (§3) |
| seals | sealings (§4) |
| t | tangential (§1) |
| th | theoretical (§3) |
| v | Volumetric (§2), |
| $v_{,built-in}$ | Constructive parameter (§2) |

## ORCID

*Roberto Capata* https://orcid.org/0000-0003-0594-0395

## REFERENCES

1. Qiu G, Liu H, Riffat S. Expanders for micro-CHP systems with organic Rankine cycle. *J Appl Thermal Eng*. 2011;31(16):3301.
2. Rohlik HE. *Analytical Determination of Radial Inflow Turbine Design Geometry for Maximum Efficiency*. NASA Technical Note; 1968.
3. Kim H, Yu J. *Design of a Scroll Expander for an ORC Applicable to a Passenger Car for Fuel Consumption Improvement*. Incheon, Korea: Department of Mechanical Engineering, University of Incheon, Korea.
4. Badr O, O'Callaghan PW, Hussein M, Probert SD. Multi-vane expanders as prime movers for low-grade energy organic Rankine-cycle engines. *J Appl Energy*. 1984;16(2):129-146.

5. Tahir MM, Yamada N, Hoshino T. Efficiency of compact organic Rankine cycle system with rotary-vane-type expander for low-temperature waste heat recovery. *Int J Environ Sci Eng*. 2010;2(1):11-16.
6. Yang B, Peng X, He Z, Guo B, Xing Z. Experimental investigation on the internal working process of a $CO_2$ rotary vane expander. *J ApplThermal Eng*. 2009;29(11):2289-2296.
7. Balje OE, Japikse D. *Turbomachines, A Guide to Design. Selection and Theory*. New York: Wiley & Sons; 1981.
8. Capata R, Pantano F. Expander selection for an onboard ORC energy recovery system. *Energy*. 2017;141(11):1084-1096.
9. Capata R, Hernandez G. Preliminary design and simulation of a turbo expanders for small rated power organic Rankine cycle. *(ORC)"–Energies 7*. 2014;11:7067-7093.
10. Stosic N, Smith KI, Kovacevic A, Aldis CA. The design of a twin-screw compressor based on a new rotor profile. *J Eng Des*. 1997;8(4):389-399.
11. Stosic N, Smith I, Brasz K, Sishtla V. The performance of a screw compressor with involute contact rotors in a low viscosity gas-liquid mixture environment. *VDI Berichte NR*. 1998;1391:279–292.
12. Zhang Y. *Experimental Study on the Performance of Single Screw Expander with 195 mm Diameter Screw*. Proceedings of 2nd International Seminar on ORC Power Systems, De Doelen, Rotterdam (NL), Oct. 7–8, 2013.
13. Margolis DL. Analytical modelling of helical screw turbines for performance prediction. *Trans ASME J Eng Power*. 1976;100:482–487.
14. Brümmer A. Energy, efficiency – waste heat utilization with screw expanders.International Compressor Engineering Conference at Purdue, July 16–19;2012.
15. Papes I, Degroote J, Vierendeels J. *3D CFD Analysis of a Twin Screw Expander for small scale ORC systems*. Proceedings of 11th World Congress on Computational Mechanics (WCCM XI – 2014), Barcelona, Spain. 2014:7207–7217. ISBN 9788494284472.
16. Sun G. The investigation of some basic geometric problems of the single screw compressor. In International Compressor Engineering Conference. 1988. Paper 630. (WCCM XI - 2014).
17. Capata R, Pantano F Expander selection for an o board ORC energy recovery system. *Energy*. 2017;141(15):1084-1096.
18. Jin G, Zhang S, Yu X. Theoretical analysis of diameter ratio of engagement pair for singe screw compressor. In International Compressor Engineering Conference. 2006. Paper 1831.
19. Lundberg A, Gianvall R. A comparison of srm and globoid type screw compressors. *Int J Refrig*. 1979;2:221-232.
20. Chen Y, Halm NP, Groll EA, Braun JE. Mathematical modeling of scroll compressors – part I: compressor process modeling. *Int J Refrig*. 2002;25:731-750.
21. Chen Y, Halm NP, Braun JE, Groll EA. Mathematical modeling of scroll compressors - part II: overall scroll compressor modeling. *Int J Refrig*. 2002;25:751-764.
22. Badr O, O'Callaghan PW, Probert SD. Multi-Vane Expanders: Geometry and Kinematics. *Appl Energy*. 1985;19:159-182.
23. Mahmoud AM. *Analytical and Experimental investigation of Rotary Vane two phase Expanders in vapor compression refrigeration systems*. PhD Thesys, University of Florida; 2008.
24. Badr O, O'Callaghan PW, Probert SD. Multi-vane expander performance: breathing characteristics. *Appl Energy*. 1985;19:241-271.
25. Badr O, O'Callaghan PW, Probert SD. Multi-vane expanders: internal-leakage losses. *Appl Energy*. 1985;20:1-46.
26. Wolgemuth CH, Olson DR. A study of breathing in vane type expanders. Proceedings of the Sixth IECEC Conference, Boston, Massachusetts, August 3–5, 1971, published by SAE.
27. Taniguchi H, Kudo K, Giedt WH, Park I, Kumazawa S. Analytical and experimental investigation of two-phase flow screw expanders for power generation. *Trans ASME J Eng Gas Turbines Power*. 1998;110:628-635.
28. Baek JS, Groll EA, Lawless PB. Development of a carbon dioxide based field deployable environmental control unit to replace HCFC-22 or HFC- 134A units. Final Report submitted to the Air Force Research Laboratory, Report #1662-1. 2002.
29. Oudkerk JF, Dickes R, Dumont O, Lemort V. Experimental performance of a piston expander in a small- scale organic Rankine cycle. *IOP Conf Ser Mater Sci Eng*. 2015;90:012066.
30. Bianchi M, Branchini L, Casari N, et al Experimental analysis of a micro-ORC driven by piston expander for low-grade heat recovery. *Appl Therm Eng*. 2019;148(5):1278-1291.
31. Dumont O, Talluri L, Fiaschi D, Manfrida G, Lemort V. *Comparison of a scroll, a screw, a roots, a piston expander and a Tesla turbine for small-scale organic Rankine cycle*. 5th International Seminar on ORC Power Systems, September 9–11, 2019, Athens, Greece.
32. Daccord R, Darmedru A, Melis J. Oil-free axial piston expander for waste heat recovery. SAE Technical Paper 2014–01-0675, 2014. SAE 2014 World Congress & Exhibition.
33. Oudkerk JF, Dickes R, Dumont O, Lemort V. Experimental performance of a piston expander in small-scale organic Rankine cycle. Proceedings of the International Conference on Compressors and their Systems; 2015.
34. Seher D, Lengenfelder T, Gerhardt J, Eisenmenger N, Hackner M, Krinn I. *Waste Heat Recovery for Commercial Vehicles with a Rankine Process, Proceeding of the, 21st Aachen Colloq*; 2012.
35. Capata R, Sciubba E. Experimental fitting of the re-scaled Balje maps for low-Reynolds radial turbomachinery. *Energies*. 2015;8(8):7986–8000.
36. Dumont O, Parthoens A, Dickes R, Lemort V Experimental investigation and optimal performance assessment of four volumetric expanders (scroll, screw, piston and roots) tested in a small-scale organic Rankine cycle system. *Energy*. 2018;165:1119-1127.
37. Weiss AP. *Volumetric expander versus turbine – which is the better choice for small ORC plants*. 3rd ASME ORC Conference, Brussels (Belgium); 2015.
38. Ziviani D, Beyene A, Venturini M. Design, analysis and optimization of a micro-CHP system based on organic Rankine cycle for ultralow grade thermal energy recovery. *J. Energy Resour Technol*. 2013;136:1.
39. Zywica G, Kaczmarczyk TZ, Ihnatowicz E. A review of expanders for power generation in small-scale organic Rankine cycle systems: performance and operational aspects. *Proc Inst Mech Eng A: J Power Energy*. 2016;230(7):669-684.


**How to cite this article:** Capata R, Pantano F. Expander design procedures and selection criterion for small rated organic rankine cycle systems. *Energy Sci Eng*. 2020;00:1–35. https://doi.org/10.1002/ese3.710